Improved resummation of post-Newtonian multipolar waveforms from circularized compact binaries

Thibault Damour,[1,2] Bala R. Iyer,[1,3] and Alessandro Nagar[1,2,4]

[1]*Institut des Hautes Etudes Scientifiques, 91440 Bures-sur-Yvette, France*
[2]*ICRANet, 65122 Pescara, Italy*
[3]*Raman Research Insitute, Bangalore 560 080, India*
[4]*INFN, Sezione di Torino, Via Pietro Giuria 1, Torino, Italy*

(Received 13 November 2008; published 3 March 2009)

We improve and generalize a resummation method of post-Newtonian multipolar waveforms from circular (nonspinning) compact binaries introduced in Refs. [1,2]. One of the characteristic features of this resummation method is to replace the usual *additive* decomposition of the standard post-Newtonian approach by a *multiplicative* decomposition of the complex multipolar waveform $h_{\ell m}$ into several (physically motivated) factors: (i) the Newtonian waveform, (ii) a relativistic correction coming from an "effective source," (iii) leading-order tail effects linked to propagation on a Schwarzschild background, (iv) a residual tail dephasing, and (v) residual relativistic amplitude corrections $f_{\ell m}$. We explore here a new route for resumming $f_{\ell m}$ based on replacing it by its ℓ-th root: $\rho_{\ell m} = f_{\ell m}^{1/\ell}$. In the extreme-mass-ratio case, this resummation procedure results in a much better agreement between analytical and numerical waveforms than when using standard post-Newtonian approximants. We then show that our best approximants behave in a robust and continuous manner as we deform them by increasing the symmetric mass ratio $\nu \equiv m_1 m_2/(m_1+m_2)^2$ from 0 (extreme-mass-ratio case) to 1/4 (equal-mass case). The present paper also completes our knowledge of the first post-Newtonian corrections to multipole moments by computing ready-to-use explicit expressions for the first post-Newtonian contributions to the odd-parity (current) multipoles.

DOI: 10.1103/PhysRevD.79.064004 PACS numbers: 04.25.Nx, 04.30.Db

I. INTRODUCTION

One of the prime targets for the currently operating network of laser interferometer gravitational wave (GW) detectors is the inspiral and merger of binary black-hole systems. To detect and interpret the GW signals from such systems one will need accurate templates to match theoretically computed signals to the noisy output of the detectors. The prime analytical framework allowing one to compute (within general relativity) the GW signal emitted by a comparable-mass binary system in the mildly relativistic regime[1] $x \sim (v/c)^2 \sim GM/(c^2 R) \ll 1$ is the post-Newtonian (PN) approximation scheme (see Ref. [3] for a review). This raises the issue of the convergence of the PN expansion, or, in practical terms, of the largest value of the PN-expansion parameter x for which the currently known PN expansions yield accurate enough GW templates. Note that, when speaking of "convergence" in this paper we shall not have in mind the mathematical question of whether the full PN expansion of, say, the (Newton-normalized) GW radiation flux, $\hat{F}^{\rm Taylor}(x) = \sum_{n=0}^{+\infty} f_n(\nu;\log x)x^n$ is a mathematically pointwise convergent series (for some fixed x belonging to some range) as $n \to +\infty$, but the more practical question of how small is the numerical difference (say in the supremum, L_∞, norm) between the currently known truncated PN expansions, say, $\hat{F}_N^{\rm Taylor} \equiv {\rm Taylor}_N \hat{F}(x) = \sum_{n=0}^{N} f_n(\nu;\log x)x^n$, for $N=3$ (3PN approximation), and the "exact" flux $\hat{F}^{\rm Exact}(x)$ in some physically relevant interval $0 < x < x_{\rm max}$, where $x_{\rm max}$ is equal or close to the value corresponding to the Last Stable (circular) Orbit (LSO). We shall then consider that some resummation method, which transforms $\hat{F}_N^{\rm Taylor}(x)$ into $\hat{F}_N^{\rm Resummed}(x)$ (say for $N=3$) is, *effective* if $\sup_{x<x^{\rm max}} |\hat{F}_N^{\rm Resummed}(x) - \hat{F}^{\rm Exact}(x)|$ is significantly smaller than $\sup_{x<x^{\rm max}} |\hat{F}_N^{\rm Taylor}(x) - \hat{F}^{\rm Exact}(x)|$ when $x_{\rm max}$ corresponds to the LSO (i.e., $x_{\rm max} = 1/6$ in the extreme-mass-ratio limit $\nu \to 0$).

It was pointed out by Cutler *et al.* [4] and Poisson [5] that the convergence (in the sense just explained) of the PN series is rather poor, especially near the LSO (i.e., when $x \simeq 1/6$) in the extreme-mass-ratio case that they considered. It was then suggested by Damour, Iyer, Sathyaprakash [6], to use *resummation methods* to extend the numerical validity of the PN expansions (at least) up to the LSO. They used several resummation techniques, and, in particular, Padé approximants. New resummation methods, aimed at extending the validity of suitably resummed PN results beyond the LSO, and up to the merger, were later introduced in the "effective-one-body" (EOB) approach and used to estimate the complete GW signal

[1]Our notation is $M \equiv m_1 + m_2$, $\mu \equiv m_1 m_2/M$, $\nu \equiv \mu/M = m_1 m_2/(m_1+m_2)^2$, $\Omega \equiv$ orbital frequency, $v \equiv (GM\Omega)^{1/3}$, $x \equiv v^2/c^2 \equiv (GM\Omega/c^3)^{2/3}$. We shall generally use x as a PN ordering parameter, and often use (without warning) units where either $c=1$ or $G=1$. We recall that a term $x^n \sim v^{2n}/c^{2n}$ is said to belong to the n-PN approximation.

emitted by inspiralling, plunging, merging, and ringing binary black-hole systems [7,8]. The EOB method has been recently improved, notably by the introduction of a new, *resummed*, 3^{+2}PN accurate[2] waveform for the $\ell = m = 2$ case [1,2]. For several, comparable-mass cases, such a waveform (married to the EOB dynamics) has been shown to agree remarkably well, both in phase and in modulus, with numerical relativity data (see [9] for review of binary black-hole numerical simulations). For instance, Ref. [10] found a phase difference smaller than ± 0.025 radians with Jena data all over the inspiral and plunge up to merger, while Ref. [2] found a remarkable amplitude agreement with published Caltech-Cornell data over the inspiral and part of the plunge. Let us note in this respect that the use of a theoretically less-accurate waveform (Newtonian-accurate multipolar waveform) still allows for a rather small phase difference, but leads to significantly larger differences in the modulus [11].

The main aim of this paper is to further improve the type of resummed multipolar waveform introduced in [1,2] for circularized (nonspinning) compact binaries. More precisely, we shall achieve here two goals: (i) on the one hand, we shall generalize the resummed $\ell = m = 2$ waveform of [1,2] to higher multipoles by using the most accurate currently known PN-expanded results [12–14] as well as the higher PN terms, which are known in the test-mass limit [15,16], and (ii) on the other hand, we shall introduce a *new resummation procedure*, which consists in considering a new theoretical quantity, denoted below as $\rho_{\ell m}(x)$, which enters the (ℓ, m) waveform (together with other building blocks, see below) only through its ℓ-th power: $h_{\ell m} \propto (\rho_{\ell m}(x))^\ell$. In this paper we shall primarily use the small-mass-ratio limit ($\nu \to 0$), in which one knows both high PN expansions of $\rho_{\ell m}(x)$ [15,16] and the exact value of $\rho_{\ell m}(x)$ from numerical studies of test particles around black holes [4,5,17], to study the quality of the convergence of $\rho_{\ell m}^{\rm Taylor}(x)$. Then we shall explore the robustness and consistency of our new approximants in the comparable-mass case.

Though we leave to later sections the precise definition of the various building blocks of our new, resummed waveform, let us already sketch here its structure. The basic idea is to write the (ℓ, m) multipolar waveform emitted by a circular[3] nonspinning compact binary as the product of several factors, namely,

$$h_{\ell m}^{(\epsilon)} = \frac{GM\nu}{c^2 R} n_{\ell m}^{(\epsilon)} c_{\ell+\epsilon}(\nu) x^{(\ell+\epsilon)/2} Y^{\ell-\epsilon,-m}\left(\frac{\pi}{2}, \Phi\right) \times \hat{S}_{\rm eff}^{(\epsilon)} T_{\ell m} e^{{\rm i}\delta_{\ell m}} \rho_{\ell m}^{\ell}. \quad (1)$$

Here, $\epsilon = 0$ for "even-parity" (mass-generated) multipoles ($\ell + m$ even), and $\epsilon = 1$ for "odd-parity" (current-generated) ones ($\ell + m$ odd); $n_{\ell m}^{(\epsilon)}$ and $c_{\ell+\epsilon}(\nu)$ are numerical coefficients; $\hat{S}_{\rm eff}^{(\epsilon)}$ is a μ-normalized effective source (whose definition comes from the EOB formalism); $T_{\ell m}$ is a resummed version [1,2] of an infinite number of "leading logarithms" entering the *tail effects* [19,20]; $\delta_{\ell m}$ is a supplementary phase (which corrects the phase effects not included in the *complex* tail factor $T_{\ell m}$), and, finally, $(\rho_{\ell m})^\ell$ denotes the ℓ-th power of the quantity $\rho_{\ell m}$, which is the new building block introduced and studied in this paper. (In previous papers [1,2] the quantity $(\rho_{\ell m})^\ell$ was denoted as $f_{\ell m}$.)

We shall discuss in quantitative details below the various facts showing that the new ingredient $\rho_{\ell m}(x)$ is a useful quantity to consider (mainly because its PN expansion has better convergence properties than the straightforward PN expansion of $h_{\ell m}$ itself). In this introductory section, we shall whet the appetite of the reader by comparing the performance of our new-resummed method, to some of the previously considered PN-based methods. For definiteness, we shall do this initial comparison at the level of the total energy flux, say F, which is related to the individual waveforms via

$$F^{(\ell_{\rm max})} = \sum_{\ell=2}^{\ell_{\rm max}} \sum_{m=1}^{\ell} F_{\ell m} = \frac{2}{16\pi G} \sum_{\ell=2}^{\ell_{\rm max}} \sum_{m=1}^{\ell} |R\dot{h}_{\ell m}|^2 = \frac{2}{16\pi G} \sum_{\ell=2}^{\ell_{\rm max}} \sum_{m=1}^{m=\ell} (m\Omega)^2 |R h_{\ell m}|^2. \quad (2)$$

Note that $F_{\ell m} = F_{\ell|m|}$ denotes the sum of two equal contributions corresponding to $+m$ and $-m$ ($m \neq 0$ as $F_{\ell 0}$ vanishes for circular orbits). This explains the explicit factor two in the last two equations above, which relate $F_{\ell m}$ to $h_{\ell m}$. It is convenient to consider the total flux F for continuity with previous studies of the convergence of PN expansions that focussed on F [4–6,17] and because of its physical importance as a measure of the radiation reaction that acts on inspiralling binaries. To be fully precise, we shall consider here the (rather accurate) approximation $F^{(6)}$ obtained by truncating the sum over ℓ in Eq. (2) beyond $\ell = 6$, and we normalize the result onto the Newtonian (i.e., quadrupolar) result $F_{22}^N = 32/5(\mu/M)^2 x^5$. In other words, we consider here the quantity $\hat{F} \equiv F^{(6)}/F_{22}^N$.

Figure 1 compares and contrasts four different ways of using the same PN information about the total Newton-normalized GW flux function $\hat{F}(v) = F(v)/F_{22}(v)$ (i.e., the same finite set of coefficients $\{f_k(\log x); 1 \leq k \leq n\}$ of the n-PN expansion of the Newton-normalized flux ${\rm Taylor}_n(\hat{F}(x)) = \sum_{k=0}^n f_k(\log x) x^k$ of the GW flux). As in

[2]The notation 3^{+2}PN refers to a "hybrid" expression which incorporates both the comparable-mass ($\nu \neq 0$) 3PN terms and the extreme-mass ratio ($\nu = 0$) 4PN and 5PN terms. See below for the precise definition of the "hybridization" procedure we use here.

[3]In this paper, we focus on the waveform emitted by exactly circular orbits (see, however, footnote 12 below). We leave to future work the study of "non-quasi-circular" corrections that must be introduced in the realistic case of inspiralling and plunging orbits (such corrections have already been introduced in the EOB approach, see [10,18]).

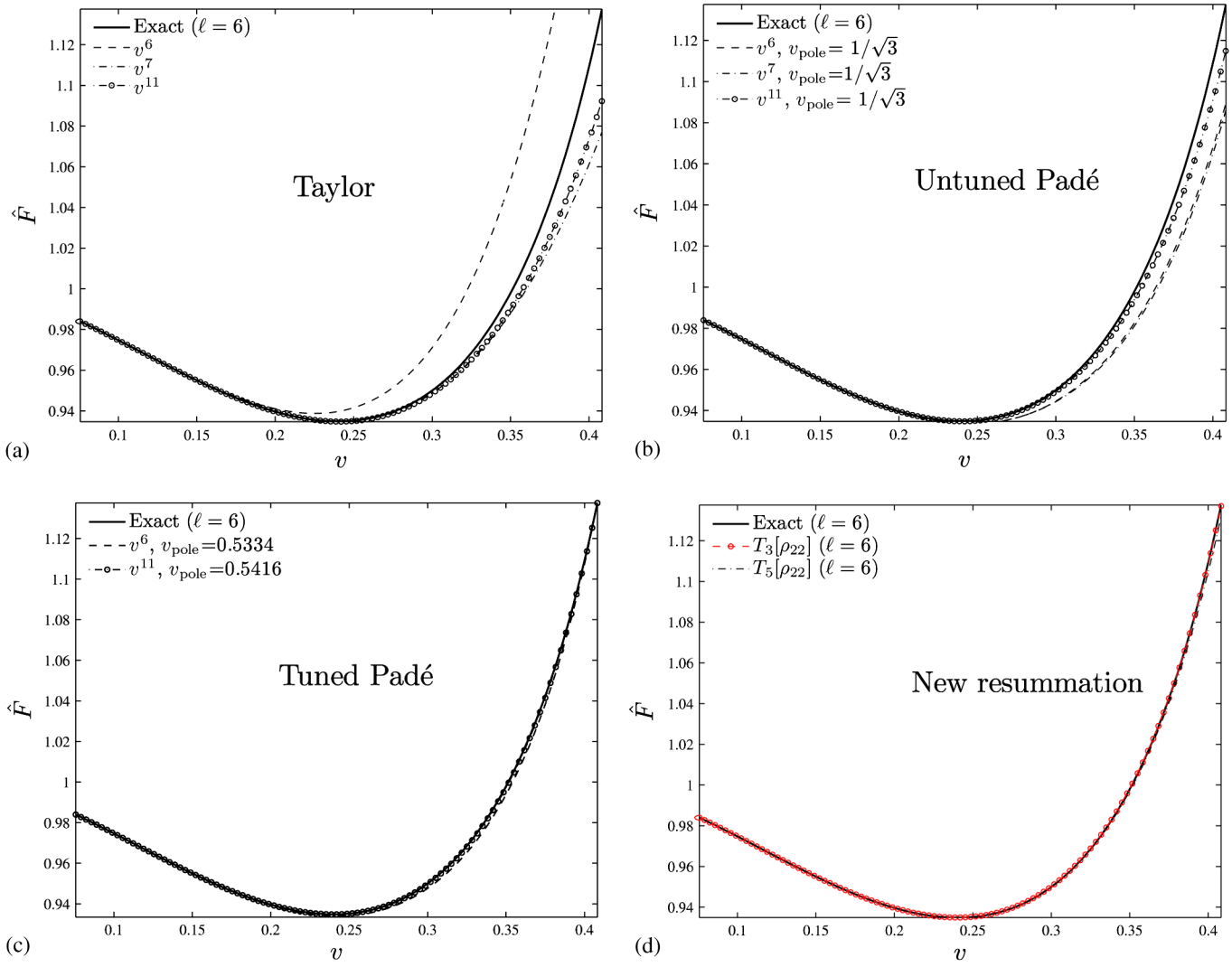

FIG. 1 (color online). Extreme-mass-ratio limit ($\nu = 0$). Comparing various resummations of the (Newton-normalized) gravitational wave energy flux: (a) standard Taylor expansion; (b) Padé resummation as proposed in Ref. [6] with $v_{\rm pole} = 1/\sqrt{3}$; (c) Padé resummation *flexing* $v_{\rm pole}$ according to the discussion of Sec. II of Ref. [2]; (d) new resummation technique based on the $\rho_{\ell m}$ functions discussed in this paper.

many previous works, we use the extreme-mass-ratio limit $\nu \to 0$ as a laboratory for devising and testing resummation procedures. Indeed, in that case, the quasicircular adiabatic description of inspiralling binaries is expected to hold up to the LSO ($x_{\rm LSO}(\nu = 0) = 1/6$) and one can compare PN-based analytical results [15,16,21] to numerical estimates of the GW flux, based on the numerical integration of some (Regge-Wheeler-Zerilli or Teukolsky) wave equation [4,17].

Panel (a) of the figure recalls the results of Refs. [4,5], namely, the rather poor convergence of the standard *Taylor approximants* of $\hat{F}(x)$ in the full interval $0 < x < x_{\rm LSO}$ where one might hope to tap the PN information. For clarity, we selected only three Taylor approximants: 3PN (v^6), 3.5PN (v^7), and 5.5PN (v^{11}). These three values suffice (by contrast with the other panels) to illustrate the rather large scatter among Taylor approximants, and the fact that, near the LSO, the convergence toward the exact value (solid line) is rather slow, and non monotonic. (See Fig. 1 in Ref. [5] and Fig. 3 of Ref. [6] for fuller illustrations of the scattered and non monotonic way in which successive Taylor expansions approach the numerical result.)

On the other hand, panel (b) recalls the results of [6], namely, the significantly better (and monotonic) way in which successive *Padé approximants* approach (in L_∞ norm on the full interval $0 < x < x_{\rm LSO}$) the numerical result. Reference [6] also showed that the observationally relevant overlaps (of both the "faithfulness" and the "effectualness" types) between analytical and numerical adiabatic signals were systematically better for Padé approximants than for Taylor ones. Note that our present

TABLE I. Errors in the flux of the two (untuned or tuned) Padé resummation procedures. From left to right, the columns report: the PN order; the difference between the resummed and the exact flux, $\Delta\hat{F} = \hat{F}^{\rm Resummed} - \hat{F}^{\rm Exact}$, at the LSO, and the L_∞ norm of $\Delta\hat{F}$, $||\Delta\hat{F}||_\infty$ (computed over the interval $0 < v < v_{\rm LSO}$), for $v_{\rm pole} = 1/\sqrt{3}$; the *flexed* value of $v_{\rm pole}$ used here; $\hat{\Delta}F$ at the LSO and the corresponding L_∞ norm (over the same interval) for the flexed value of $v_{\rm pole}$.

PN order	$\Delta\hat{F}^{1/\sqrt{3}}_{\rm LSO}$	$\|\|\Delta\hat{F}\|\|^{1/\sqrt{3}}_\infty$	$v_{\rm pole}$	$\Delta\hat{F}^{v_{\rm pole}}_{\rm LSO}$	$\|\|\Delta\hat{F}\|\|^{v_{\rm pole}}_\infty$
3 (v^6)	−0.048	0.048	0.5334	7.06×10^{-5}	0.00426
3.5 (v^7)	−0.051	0.051	0.5425	5.50×10^{-5}	0.00429
5.5 (v^{11})	−0.022	0.022	0.5416	2.52×10^{-5}	0.000 854

panel (b) is slightly different from the corresponding results in panel (b) of Fig. 3 in [6] [in particular, the present panel (b) exhibits a better convergence of the v^{11} curve]. This difference is due to the new treatment of the logarithmic terms $\propto \log x$. Instead of factoring them out in front as proposed in [6], we consider them here (following [2]) as being part of the "Taylor coefficients" $f_n(\log x)$ when Padéing the flux function. Note also that panel (b) follows Ref. [6] in introducing a pole in the resummed flux $\hat{F}(v)$ located at the value $v^{(\nu=0)}_{\rm pole} = 1/\sqrt{3}$.

By contrast, panel (c) of the figure illustrates the remarkable improvement in the (L_∞) closeness between $\hat{F}^{\rm Padé\text{-}resummed}(v)$ and $\hat{F}^{\rm Exact}(v)$ obtained, as recently suggested by Damour and Nagar [2] (following ideas originally introduced in Ref. [22]), by suitably flexing the value of $v_{\rm pole}$. As proposed in Ref. [2], $v_{\rm pole}$ is tuned until the difference between the resummed and the exact flux at the LSO is zero (or at least smaller than 10^{-4}). The resulting closeness between the exact and tuned-resummed fluxes is so good (compared to the previous panels, where the differences were clearly visible) that we need to complement panel (c) of Fig. 1 with Table I. This table compares in a quantitative way the result of the "untuned" Padé resummation ($v_{\rm pole} = 1/\sqrt{3}$) of Ref. [6] to the result of the "$v_{\rm pole}$-tuned" Padé resummation of Ref. [2]. Defining the function $\Delta\hat{F}(v; v_{\rm pole}) = \hat{F}^{\rm Resummed}(v; v_{\rm pole}) - \hat{F}^{\rm Exact}(v)$ measuring the difference between a resummed and the exact energy flux, Table I lists both the values of $\Delta\hat{F}$ at $v = v_{\rm LSO}$ and its L_∞ norm on the interval $0 < v < v_{\rm LSO}$ for both the untuned and tuned cases. Note, in particular, how the $v_{\rm pole}$-flexing approach permits to reduce the L_∞ norm over this interval by more than an order of magnitude with respect to the untuned case. Note that the closeness between the tuned flux and the exact one is remarkably good (4.3×10^{-3}) already at the 3PN level.

Finally, panel (d) of Fig. 1 illustrates the even more remarkable improvement in the closeness between $\hat{F}^{\rm New\text{-}resummed}$ and $\hat{F}^{\rm Exact}$ obtained by means of the new resummation procedure proposed in this paper. More precisely, panel (d) plots two examples of fluxes obtained from our new $\rho_{\ell m}$ representation, Eq. (1), for the individual multipolar waveforms $h_{\ell m}$ in the sum Eq. (2). These two examples differ in the choice of approximants for the $\ell = m = 2$ partial wave. One example uses for ρ_{22} its 3PN Taylor expansion, $T_3[\rho_{22}]$, while the other one uses its 5PN Taylor expansion, $T_5[\rho_{22}]$. All the other partial waves are given by their maximum known Taylor expansion. Note that the fact that we use here for the $\rho_{\ell m}$'s some straightforward Taylor expansions does not mean that our new procedure is not a resummation technique. Indeed, the defining resummation features of our procedure have four sources: (i) the factorization of the PN corrections to the waveforms into four different blocks, namely, $\hat{S}^{(\epsilon)}_{\rm eff}$, $T_{\ell m}$, $e^{i\delta_{\ell m}}$, and $\rho^\ell_{\ell m}$ in Eq. (1); (ii) the fact the $\hat{S}^{(\epsilon)}_{\rm eff}$ is by itself a resummed source whose PN expansion would contain an infinite number of terms; (iii) the fact that the tail factor is a closed form expression [see Eq. (19) below] whose PN expansion also contains an infinite number of terms and (iv) the fact that we have replaced the Taylor expansion of $f_{\ell m} \equiv \rho^\ell_{\ell m}$ by that of its ℓ-th root, namely, $\rho_{\ell m}$.

Even more so than in the $v_{\rm pole}$-tuned case of panel (c), the closeness between analytical and exact results exhibited by the "new-resummed" case of panel (d) is so good that it is undistinguishable by eye. We therefore complement panel (d) by displaying in Fig. 2 the residual differences $\Delta\hat{F}(v) = \hat{F}^{\rm New\text{-}resummed}(v) - \hat{F}^{\rm Exact}(v)$. We included in Fig. 2 a third curve corresponding to the case where we further resum our "new-resummed" flux by using for (the 5PN accurate) ρ_{22} its near-diagonal (2, 3) Padé approximant, say $P^2_3\{T_5[\rho_{22}(x)]\}$, instead of its Taylor expansion. (The other $\rho_{\ell m}$'s being still used in Taylor-expanded form). Note that the difference $\Delta\hat{F}$ at the LSO is $\approx 4.5 \times 10^{-4}$ when using $T_3[\rho_{22}]$, is -5.7×10^{-3} when using $T_5[\rho_{22}]$ and is $+1.6 \times 10^{-3}$ when using $P^2_3\{T_5[\rho_{22}(x)]\}$. Note that these numbers are in the same ballpark as the v^{11}-accurate $v_{\rm pole}$-tuned result (8.5×10^{-4}) quoted in Table I. Discarding the very small difference corresponding to the 3PN-accurate T_3 case as being probably accidental we conclude that using the normal, near-diagonal[4] Padé resummation of *only* the leading multipolar contribution ρ_{22} has the effect of significantly improving the agreement with the exact result (compare the two 5PN-accurate curves, $T_5[\rho_{22}]$ and $P^2_3\{T_5[\rho_{22}(x)]\}$, in Fig. 2). We therefore expect that Padéing some of the higher multipoles will

[4]We will explore other Padé approximants of ρ_{22} below.

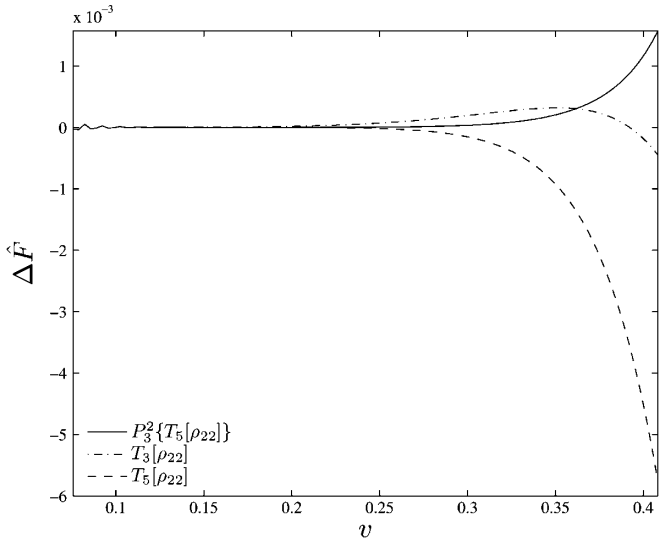

FIG. 2. Extreme-mass-ratio limit ($\nu = 0$). Complement to panel (d) of Fig. 1. Difference between the resummed and exact energy flux, for different approaches to the resummation of the ρ_{22} function. See text for explanations.

further improve the agreement between the energy fluxes. Note also, in passing, that the new resummation procedure explored here is more "predictive" than the $v_{\rm pole}$-flexing technique in that it does not need to rely on the knowledge of the exact answer. We will also show below that it is "robust" under the deformation brought about by increasing the symmetric mass ratio ν from 0 up to its maximal value $1/4$.

This paper is organized as follows: in Sec. II we explicitly define the building blocks entering the resummation of the gravitational waveform. Section III analyzes the performance of this resummation procedure in the extreme-mass-ratio ($\nu \to 0$) case, while Sec. IV considers the comparable-mass case ($\neq 0$). We present some concluding remarks in Sec. V. The paper is completed by three appendices, which present many useful formulas that complete the discussion of the main text. In particular, Appendix A provides the first explicit, ready-to-use expression for the 1-PN corrections to the symmetric-trace-free (STF) current-multipole moments and to the corresponding spherical-harmonics odd-parity multipoles for arbitrary ℓ and m.

II. DEFINING THE BUILDING BLOCKS OF THE RESUMMATION OF THE MULTIPOLAR GRAVITATIONAL WAVEFORM

Let us now explicitly define each of the building blocks of our new-resummed waveform, Eq. (1). Note that our methodology differs from the PN methodology in a basic way. The PN approach consists in writing any relativistic quantity as a *sum* of various contributions starting with the so-called Newtonian approximation. In other words, a PN-expanded multipolar waveform has the structure $h_{\ell m} = h^N_{\ell m} + h^{\rm 1PN}_{\ell m} + h^{\rm 1.5PN}_{\ell m} + \ldots$. By contrast to this *additive* approach we will use here, as advocated in Refs. [1,2], a *multiplicative* approach in which any relativistic quantity is decomposed as a *product* of various contributions.[5] One of the factors of this multiplicative decomposition will be the Newtonian waveform, $h^N_{\ell m}$. Some of the other factors are chosen so as to best capture part of the essential physics contained in the waveform. The remaining factors will then resum the subleading effects that have not been included in the previous ones. First of all, it is convenient to introduce the following notation

$$h_{\ell m} = h^{(N,\epsilon)}_{\ell m} \hat{h}^{(\epsilon)}_{\ell m}, \tag{3}$$

where $h^{(N,\epsilon)}_{\ell m}$ represents the Newtonian contribution and $\hat{h}^{(\epsilon)}_{\ell m}$ the product of all the other factors in our multiplicative decomposition. As all these other factors represent resummed version of PN corrections (of the type $1 + \mathcal{O}(x)$) their product will also have the structure $\hat{h}^{(\epsilon)}_{\ell m} = 1 + \mathcal{O}(x)$.

A. The Newtonian multipolar waveform

Though all the work in this paper will focus on the resummation of the PN-correcting factor $\hat{h}^{(\epsilon)}_{\ell m}$, let us, for completeness, recall the well-known [12,14,23] structure of the Newtonian multipolar waveform,[6] here considered for the adiabatic circular case. The Newtonian contribution for circular orbits is, for given (ℓ, m), a function of $x \equiv (GM\Omega/c^3)^{2/3}$ and the two mass ratios $X_1 = m_1/M$ and $X_2 = m_2/M$[7]

$$h^{(N,\epsilon)}_{\ell m} = \frac{GM\nu}{c^2 R} n^{(\epsilon)}_{\ell m} c_{\ell+\epsilon}(\nu) x^{(\ell+\epsilon)/2} Y^{\ell-\epsilon,-m}\left(\frac{\pi}{2}, \Phi\right). \tag{4}$$

Here, ϵ denotes the parity of the multipolar waveform, i.e., even ($\epsilon = 0$) for mass-generated multipoles and odd ($\epsilon = 1$) for current-generated ones. In the circular case, ϵ is equal to the parity of the sum $\ell + m$: $\epsilon = \pi(\ell + m)$. In other words $\epsilon = 0$ when $\ell + m$ is even, and $\epsilon = 1$ when $\ell + m$ is odd. The $Y^{\ell m}(\theta, \phi)$ are the usual scalar spherical harmonics,[8] while

[5]This multiplicative approach can be naturally applied to the multipolar waveform $h_{\ell m}$, which is a *complex number*.

[6]We mostly follow here the conventions of Refs. [12,23], except that we take into account some of the simplifications used in [14]. Note the presence of a factor $1/\sqrt{2}$ in the relation between the (ℓ, m) Newtonian waveform and the corresponding (ℓ, m) radiative multipoles: $Rh^{\rm even}_{\ell m} = (G/\sqrt{2})U_{\ell m} = (G/\sqrt{2})I^{(\ell)}_{\ell m}$ for mass multipoles and $Rh^{\rm odd}_{\ell m} = -{\rm i}(G/\sqrt{2})V_{\ell m} = -{\rm i}(G/\sqrt{2})S^{(\ell)}_{\ell m}$ for current multipoles.

[7]Note that $X_1 + X_2 = 1$, $X_1 X_2 = \nu$, where ν is the symmetric mass ratio $\nu \equiv m_1 m_2/(m_1 + m_2)^2$, while $X_1 - X_2 = {\rm sign}(m_1 - m_2)\sqrt{1 - 4\nu}$, where the sign depends whether $m_1 > m_2$ or the reverse.

[8]We use the $Y_{\ell m}$'s defined in Eqs. (2.7) and (2.8) of Ref. [23], or equivalently by the $s = 0$ case of Eqs. (4) and (5) of Ref. [12].

$$n^{(0)}_{\ell m} = (\mathrm{i}m)^\ell \frac{8\pi}{(2\ell+1)!!}\sqrt{\frac{(\ell+1)(\ell+2)}{\ell(\ell-1)}}, \tag{5}$$

$$n^{(1)}_{\ell m} = -(\mathrm{i}m)^\ell \frac{16\pi\mathrm{i}}{(2\ell+1)!!}\sqrt{\frac{(2\ell+1)(\ell+2)(\ell^2-m^2)}{(2\ell-1)(\ell+1)\ell(\ell-1)}}, \tag{6}$$

are (ν-independent) numerical coefficients. Finally, the ν-dependent coefficients $c_{\ell+\epsilon}(\nu)$ (such that $|c_{\ell+\epsilon}(\nu=0)|=1$), can be expressed in terms of ν (as in Refs. [12,14]), although it is more conveniently written in terms of the two mass ratios X_1 and X_2 in the form[9]

$$\begin{aligned} c_{\ell+\epsilon}(\nu) &= X_2^{\ell+\epsilon-1} + (-)^{\ell+\epsilon} X_1^{\ell+\epsilon-1} \\ &= X_2^{\ell+\epsilon-1} + (-)^m X_1^{\ell+\epsilon-1}. \end{aligned} \tag{7}$$

In the second form of the equation we have used the fact that, as $\epsilon = \pi(\ell+m)$, $\pi(\ell+\epsilon)=\pi(m)$.

B. The first three factors in the multiplicative decomposition of the PN fractional correction $\hat{h}^{(\epsilon)}_{\ell m}$

Let us recall that, in the comparable-mass case ($\nu \neq 0$), the $\hat{h}^{(\epsilon)}_{\ell m}$-PN correction can be computed within the perturbative multipolar-post-Minkowskian (MPM) formalism [3,19,20], while in the test-mass limit ($\nu \to 0$) it can be obtained by black-hole perturbation theory [15,16,24,25].

The final result is that $\hat{h}^{(\epsilon)}_{\ell m}$ is given by a PN expansion of the form $\hat{h}_{\ell m} = 1 + h_1 x + h_{1.5} x^{3/2} + \ldots$. For comparable-mass circularized compact binaries, the partial wave which is known with the highest PN accuracy is the leading even-parity quadrupolar wave $\hat{h}_{22}$, which is known to fractional 3PN accuracy [2,12,14,26]. Note that Ref. [14] provides $h_{\ell m}$ half a PN order more accurately than Ref. [12] for multipolar orders $(\ell, m) = (2,1)$, (3, 3), (3, 2), (3, 1), (4, 3), (4, 1), (5, 5), (5, 3), and (5, 1). This information is fully employed in this work. In the extreme-mass-ratio case, the partial waves are known with even higher PN accuracy. For instance, $\hat{h}_{22}$ is known to 5.5PN [15,16] and other multipoles to accuracies consistent with 5.5PN GW flux. As explained later, this information is also appropriately exploited in our construction.

As indicated above, the resummation method we shall use here consists in (i) decomposing the PN-correction factor $\hat{h}^{(\epsilon)}_{\ell m} = 1 + h_1 x + h_{1.5} x^{3/2} + \ldots$ into the *product of four factors*, each of which has a similar PN-expansion, $1 + \mathcal{O}(x)$, namely,

$$\hat{h}^{(\epsilon)}_{\ell m} = \hat{S}^{(\epsilon)}_{\rm eff} T_{\ell m} e^{\mathrm{i}\delta_{\ell m}} \rho^\ell_{\ell m}, \tag{8}$$

and then (ii) resumming separately each factor.

The choice of these various factors is based on our physical intuition of the main physical effects entering the final waveform. The first factor is motivated by thinking about the form of the equation satisfied by each partial wave in the (circular) test-mass limit: indeed in this limit $\hat{h}_{\ell m}$ is the asymptotic value (at spatial infinity) of a solution of a (frequency-domain) wave equation of the Regge-Wheeler-Zerilli type (see, e.g., Ref. [27]). The source term appearing on the right-hand side of this equation is a linear combination of terms linear in the stress-energy tensor $T_{\mu\nu}$ of a test particle of mass μ moving around a black hole of mass M. As the effective-one-body method has shown that the dynamics of comparable-mass black holes can be mapped onto the dynamics of an effective particle of mass μ moving in some effective metric (which reduces to the Schwarzschild metric of mass M when $\nu \to 0$), it is natural to introduce (both when $\nu \to 0$ and $\nu \neq 0$) effective source terms in the partial waves made up from the important dynamical characteristics of the EOB dynamics, namely, the effective EOB Hamiltonian $H_{\rm eff}$ and the EOB angular momentum $\mathcal{J}$. This motivates us to define as first factor in $\hat{h}_{\ell m}$ an effective source term $S^{(\epsilon)}_{\rm eff}$ proportional either to $H_{\rm eff}$ or $\mathcal{J}$. Note that this idea of factoring $H_{\rm eff}$ or $\mathcal{J}$ from the wave amplitude is similar to the suggestion of Ref. [6] of factoring out a pole in the energy flux. Indeed, the analytical continuation in x of the flux function $F(x)$ below the LSO inherits, in the $\nu \to 0$ limit, a simple pole from the fact that $F(x)$ is proportional to the square[10] of the energy of the "rotating source" (see discussion p. 893 of [6]).

Our second factor is motivated by thinking about the structure of the "transfer" function relating (in the comparable-mass case) the far-zone GW amplitude $h_{\ell m}$ to the near-zone one. If we keep, in the full Einstein equations considered outside the binary system, only the terms coupling the instantaneous "monopolar" Arnowitt-Deser-Misner (ADM) mass of the system, $M_{\rm ADM} = M +$ binding energy $= H_{\rm real}$, to the multipolar wave amplitude, we get (in the circular approximation and in the Fourier domain) a Schrödinger-type equation, for each multipole order ℓ, containing a potential $V_\ell(r)$ whose leading behavior as $r \to \infty$ is dominated by two effects: (i) the $\ell(\ell+1)/r^2$ centrifugal barrier, and (ii) a more slowly decreasing term $\sim -4M_{\rm ADM}\omega^2/r$ coming from the coupling to a curved (Schwarzschild-like) monopolar background metric. One can solve this leading-order equation by means of

[9] When expressing $c_{\ell+\epsilon}(\nu)$ as an explicit function of ν, as in Ref. [12], it is useful to note that $c_{\ell+\epsilon}(\nu)$ vanishes in the equal-mass case when $\ell+\epsilon$ is odd, which is equivalent (given that $\epsilon = \pi(\ell+m)$ for circular orbits), to m being odd. In such cases one can factor out, as in Refs. [12,14], from $c_{\ell+\epsilon}(\nu)$ a factor $\Delta \equiv X_1 - X_2 = \mathrm{sign}(m_1-m_2)\sqrt{1-4\nu}$. The $c_\ell(\nu)$ in this paper are the same as the $s_\ell(\nu)$ in [14]. Note however that in Appendix A of Ref. [12], in the second line above Eq. (A7), the definition of d_ℓ should include a supplementary factor $m/\delta m = 1/(X_1 - X_2)$ on the right-hand side.

[10] Note that in the $\nu \to 0$ limit both $H_{\rm eff}$ and $\mathcal{J}$ have a square-root singularity $\propto 1/\sqrt{1-3x}$ at the light ring. See, e.g., Eqs. (56)–(58) below.

Coulomb wave functions. When doing this, it is found that each asymptotic partial wave is related to its corresponding near-zone expression by a certain "tail" factor $T_{\ell m}$. It can be checked that, in the comparable-mass case, this tail factor represents the resummation of the infinite number of leading logarithms (see Eqs. (7)–(9) in [2]) that appear when computing asymptotic multipolar waves in the MPM formalism [3,19,20]. Having so factorized two of the main physical effects entering $\hat{h}_{\ell m}$, we define the two other factors as the phase, $e^{i\delta_{\ell m}}$ and the modulus, $f_{\ell m}$ of the remaining quotiented Newton-normalized waveform. In this subsection we discuss in detail the first three factors, postponing to the following subsection the last one, namely, the modulus $f_{\ell m}$.

Let us start by discussing the structure of the $\hat{S}^{(\epsilon)}_{\rm eff}$ and $T_{\ell m}$ factors. In the even-parity case (corresponding to mass moments), since the leading-order source of gravitational radiation is given by the energy density, it is natural to define

$$\hat{S}^{(0)}_{\rm eff}(x) = \hat{H}_{\rm eff}(x) \qquad \ell + m \quad \text{even}. \tag{9}$$

Here, $\hat{H}_{\rm eff}$ is the *effective* EOB Hamiltonian (per unit μ mass), that we shall restrict here along the sequence of EOB circular orbits. When $\nu \to 0$, $\hat{H}_{\rm eff}$ reduces to the usual conserved energy of a test-mass μ in a Schwarzschild background of mass M [see Eq. (56) below].

The explicit expression of $\hat{H}_{\rm eff}$, along circular orbits, as a function of the frequency parameter x, cannot be written in closed form [7,8]. However, it can be written in parametric form in terms of the EOB inverse radius parameter[11] $u = 1/r$. More precisely, we have

$$\hat{H}_{\rm eff} = \frac{H_{\rm eff}}{\mu} = \sqrt{A(u)(1 + j^2u^2)} \qquad \text{(circular orbits)}, \tag{10}$$

where $u = 1/r$, and where $A(u)(\equiv -g^{\rm effective}_{00}(r))$ is the crucial EOB radial potential and $j = \mathcal{J}/(\mu GM)$ is the (dimensionless) angular momentum along circular orbits. We recall that the PN expansion of $A(u)$ has the form

$$A^{\rm Taylor}(u) = 1 - 2u + 2\nu u^3 + \left(\frac{94}{3} - \frac{41}{32}\pi^2\right)\nu u^4 + a_5\nu u^5 + \mathcal{O}(\nu u^6), \tag{11}$$

where the u^4 term corresponds to 3PN contributions to the EOB dynamics [28] and where we have parametrized the presence of yet uncalculated 4PN (and higher) contributions to $A(u)$ by adding a term $+a_5(\nu)u^5$ with the simple form $a_5(\nu) = a_5\nu$. As in previous EOB work, we shall not use the Taylor-expanded function $A^{\rm Taylor}(u)$, but replace it by a suitably Padé resummed function $A(u)$.

[11] As usual in EOB work, we use dimensionless variables, notably $r = Rc^2/GM$, where R is the EOB Schwarzschild-like radial coordinate.

The circular orbits in the EOB formalism are determined by the condition $\partial_u\{A(u)[1 + j^2u^2]\} = 0$, which leads to the following parametric representation of the squared angular momentum:

$$j^2(u) = -\frac{A'(u)}{(u^2A(u))'} \qquad \text{(circular orbits)}, \tag{12}$$

where the prime denotes d/du. Inserting this u-parametric representation of j^2 in Eq. (10) defines the u-parametric representation of the effective Hamiltonian $\hat{H}_{\rm eff}(u)$. We can then obtain (at least numerically) $\hat{H}_{\rm eff}$ as a function of x by eliminating u between $\hat{H}_{\rm eff}(u)$ and the corresponding u-parametric representation of the frequency parameter $x = (GM\Omega/c^3)^{2/3}$ obtained by the angular Hamilton equation of motion in the circular case

$$M\Omega(u) = \frac{1}{\mu}\frac{\partial H_{\rm real}}{\partial j} = \frac{MA(u)j(u)u^2}{H_{\rm real}\hat{H}_{\rm eff}}, \tag{13}$$

where $H_{\rm real}$ denotes the real EOB Hamiltonian

$$H_{\rm real} = M\sqrt{1 + 2\nu(\hat{H}_{\rm eff} - 1)}. \tag{14}$$

While in the even-parity case we shall factor out $\hat{H}_{\rm eff}(x)$ as a "source term," in the odd-parity one we explored two, equally motivated, possibilities. The first one consists simply in still factoring $\hat{H}_{\rm eff}(x)$; i.e., in defining

$$\hat{S}^{(1,H)}_{\rm eff} = \hat{H}_{\rm eff}(x) \qquad \ell + m \quad \text{odd}. \tag{15}$$

The second one consists in factoring the angular momentum $\mathcal{J}$. Indeed, the angular momentum density $\epsilon_{ijk}x^j\tau^{0k}$ enters as a factor in the (odd-parity) current moments, and $\mathcal{J}$ occurs (in the small-ν limit) as a factor in the source of the Regge-Wheeler-Zerilli odd-parity multipoles. This leads us to define as a second possibility

$$\hat{S}^{(1,J)}_{\rm eff} = \hat{j}(x) \equiv x^{1/2}j(x) \qquad \ell + m \quad \text{odd}, \tag{16}$$

where $\hat{j}$ denotes what can be called the "Newton-normalized" angular momentum, namely, the ratio $\hat{j}(x) = j(x)/j_N(x)$ with $j_N(x) = 1/\sqrt{x}$. [This Newtonian normalization being such that $\hat{j}(x) = 1 + \mathcal{O}(x)$.] We will compare below the performances of these two possible choices. Note that the PN expansions of these two possible sources start as

$$\hat{H}_{\rm eff}(x) = 1 - \tfrac{1}{2}x + \mathcal{O}(x^2), \tag{17}$$

$$\hat{j}(x) = 1 + \left(\frac{3}{2} + \frac{\nu}{6}\right)x + \mathcal{O}(x^2). \tag{18}$$

The second building block in our factorized decomposition is the "tail factor" $T_{\ell m}$ (introduced in Refs. [1,2]). As mentioned above, $T_{\ell m}$ is a resummed version of an infinite numbers of "leading logarithms" entering the transfer function between the near-zone multipolar wave and the

far-zone one, due to *tail effects* linked to its propagation in a Schwarzschild background of mass $M_{\rm ADM} = H_{\rm real}$. Its explicit expression reads

$$T_{\ell m} = \frac{\Gamma(\ell + 1 - 2i\hat{\hat{k}})}{\Gamma(\ell + 1)} e^{\pi\hat{\hat{k}}} e^{2i\hat{\hat{k}}\log(2kr_0)}, \tag{19}$$

where $r_0 = 2GM$ and $\hat{\hat{k}} \equiv GH_{\rm real} m\Omega$ and $k \equiv m\Omega$. Note that $\hat{\hat{k}}$ differs from k by a rescaling involving the *real* (rather than the *effective*) EOB Hamiltonian, Eq. (14).

The tail factor $T_{\ell m}$ is a complex number, which already takes into account some of the dephasing of the partial waves as they propagate out from the near zone to infinity. However, as the tail factor only takes into account the leading logarithms, one needs to correct it by a complementary dephasing term, $e^{i\delta_{\ell m}}$, linked to subleading logarithms and other effects. This subleading phase correction can be computed as being the phase $\delta_{\ell m}$ of the complex ratio between the PN-expanded $\hat{h}^{(\epsilon)}_{\ell m}$ and the above defined source and tail factors. In the comparable-mass case ($\nu \neq 0$), the 3PN δ_{22} phase correction to the leading quadrupolar wave was computed in Ref. [2] (see also Ref. [1] for the $\nu = 0$ limit). For the subleading partial waves, we computed the other $\delta_{\ell m}$'s to the highest possible PN accuracy by starting from the currently known 3PN-accurate ν-dependent waveform [14]. Our explicit results read

$$\delta_{22} = \frac{7}{3} y^{3/2} + \frac{428\pi}{105} y^3 - 24\nu\bar{y}^{5/2}, \tag{20}$$

$$\delta_{21} = \frac{2}{3} y^{3/2} - \frac{493\nu}{42} \bar{y}^{5/2}, \tag{21}$$

$$\delta_{33} = \frac{13}{10} y^{3/2} - \frac{80897}{2430} \nu\bar{y}^{5/2}, \tag{22}$$

$$\delta_{32} = \frac{10 + 33\nu}{15(1 - 3\nu)} y^{3/2}, \tag{23}$$

$$\delta_{31} = \frac{13}{30} y^{3/2} - \frac{17\nu}{10} \bar{y}^{5/2}, \tag{24}$$

$$\delta_{44} = \frac{112 + 219\nu}{120(1 - 3\nu)} y^{3/2}, \tag{25}$$

$$\delta_{43} = \frac{486 + 4961\nu}{810(1 - 2\nu)} y^{3/2}, \tag{26}$$

$$\delta_{42} = \frac{7(1 + 6\nu)}{15(1 - 3\nu)} y^{3/2}, \tag{27}$$

$$\delta_{41} = \frac{2 + 507\nu}{10(1 - 2\nu)} y^{3/2}, \tag{28}$$

$$\delta_{55} = \frac{96875 + 857528\nu}{131250(1 - 2\nu)} y^{3/2}. \tag{29}$$

Here, following Ref. [2], we define $y \equiv (H_{\rm real}\Omega)^{2/3}$, which gathers together relativistic corrections (like those entering the tail) that depend on the instantaneous ADM mass of the system, namely, $H_{\rm real}$, rather than the total "mechanical mass" M. Concerning the last $\bar{y}^{5/2}$ corrections,[12] it is not clear whether they are more linked to the ADM mass or to the mechanical mass. This is why we use the notation $\bar{y}$, meaning that it could be replaced either by x or y [note that in Ref. [2] we chose $\bar{y} = x$ inside the $-24\nu\bar{y}^{5/2}$ correction to δ_{22}, Eq. (11) there]. Indeed, these 2.5PN terms are not known to 1PN fractional accuracy because we rely here on the available 3PN (and not 3.5PN) accurate results of [14].

In the extreme-mass-ratio limit $\nu \to 0$, the information needed to compute some of the higher-order PN corrections to the $\delta_{\ell m}$'s is contained in the results of Ref. [15]. We leave to future work the task of exploiting this information to complete the above ν-dependent $\delta_{\ell m}$'s with higher-order $\nu = 0$ corrections. In addition we shall leave here the $\delta_{\ell m}$'s in Taylor-expanded form. We leave to future work an eventual comparison between numerically determined phases and (possibly resummed) analytic ones.

C. The fourth factor in the multiplicative decomposition of the PN fractional correction $\hat{h}^{(\epsilon)}_{\ell m}$

The fourth and last factor in the multiplicative decomposition, Eq. (8), can be computed as being the modulus $f_{\ell m}$ of the complex ratio between the PN-expanded $\hat{h}^{(\epsilon)}_{\ell m}$ and the above defined source and tail factors. In the comparable-mass case ($\nu \neq 0$), the f_{22} modulus correction to the leading quadrupolar wave was computed in Ref. [2] (see also Ref. [1] for the $\nu = 0$ limit). For the subleading partial waves, we compute here the other $f_{\ell m}$'s to the highest possible PN accuracy by starting from the currently known 3PN-accurate ν-dependent waveform [14]. In addition, as originally proposed in Ref. [2], to reach greater accuracy the $f_{\ell m}(x;\nu)$'s extracted from the 3PN-accurate $\nu \neq 0$ results are complemented by adding higher-order contributions coming from the $\nu = 0$ results [15,16]. In the particular f_{22} case discussed in [2], this amounted to adding 4PN and 5PN $\nu = 0$ terms. This hybridization procedure is here systematically pursued for all the other multipoles, using the 5.5PN accurate calculation of the multipolar decomposition of the gravitational wave energy flux done in Refs. [15,16]. It is worth emphasizing at this stage that our hybridization procedure is *not* equivalent to the straightforward hybrid sum ansatz, $\tilde{h}_{\ell m} = \tilde{h}^{\rm known}_{\ell m}(\nu) + \tilde{h}^{\rm higher}_{\ell m}(\nu = 0)$ (where $\tilde{h}_{\ell m} \equiv h_{\ell m}/\nu$) that one may have

[12] Note that these $\mathcal{O}(\bar{y}^{5/2})$ corrections in $\delta_{\ell m}$ are the only terms in the wave amplitude that we use here, which go beyond the strict "circular limit" in that they include contributions proportional to the (radiation-reaction-driven) time derivatives of the orbital radius, or of the orbital frequency.

chosen to implement. The detailed definition of the hybridization procedure that we use, as well as the reasons why we think that our procedure is better than others, will be explained below.

In the even-parity case, the determination of the modulus $f_{\ell m}$ is unique. In the odd-parity case, it depends on the choice of the source which, as explained above, can be either connected to the effective energy or to the angular momentum. We will consider both cases and distinguish them by adding either the label H or $\mathcal{J}$ of the corresponding $f_{\ell m}$. Note, in passing, that, since in both cases the factorized effective source term ($H_{\rm eff}$ or $\mathcal{J}$) is a real quantity, the phases $\delta_{\ell m}$'s are the same.

The above explained procedure defines the $f_{\ell m}$'s as Taylor-expanded PN series of the type

$$f_{\ell m}(x;\nu) = 1 + c_1^{f_{\ell m}}(\nu)x + c_2^{f_{\ell m}}(\nu)x^2 + c_3^{f_{\ell m}}(\nu, \log(x))x^3 + \ldots \tag{30}$$

Note that one of the virtues of our factorization is to have separated the half-integer powers of x appearing in the usual PN expansion of $h_{\ell m}^{(\epsilon)}$ from the integer powers, the tail factor, together with the complementary phase factor $e^{i\delta_{\ell m}}$, having absorbed all the half-integer powers.

We have computed all the $f_{\ell m}$'s (both for the H and $\mathcal{J}$ choices) up to the highest available (ν dependent or not) PN accuracy. In the formulas for the $f_{\ell m}$'s given below we "hybridize" them by adding to the known ν-dependent coefficients $c_n^{f_{\ell m}}(\nu)$ in Eq. (30) the $\nu = 0$ value of the higher-order coefficients $c_{n'}^{f_{\ell m}}(\nu = 0)$. The 1PN-accurate $f_{\ell m}$'s for $\ell + m$ even and—thanks to the new results for 1PN current multipoles obtained in Appendix A for arbitrary ℓ—also for $\ell + m$ odd can be written down for all ℓ. In Appendix B we list the complete results for the $f_{\ell m}$'s that are known with an accuracy higher than 1PN. Here, for illustrative purposes, we quote only the lowest $f_{\ell m}^{\rm even}$ and $f_{\ell m}^{{\rm odd},J}$ up to $\ell = 3$ included.

$$f_{22}(x;\nu) = 1 + \frac{1}{42}(55\nu - 86)x + \frac{(2047\nu^2 - 6745\nu - 4288)}{1512}x^2 + \left(\frac{114\,635\nu^3}{99\,792} - \frac{22\,7875\nu^2}{33\,264} + \frac{41}{96}\pi^2\nu - \frac{34\,625\nu}{3696} - \frac{856}{105}\text{eulerlog}_2(x) + \frac{21\,428\,357}{727\,650}\right)x^3 + \left(\frac{36\,808}{2205}\text{eulerlog}_2(x) - \frac{5\,391\,582\,359}{198\,648\,450}\right)x^4 + \left(\frac{458\,816}{19\,845}\text{eulerlog}_2(x) - \frac{93\,684\,531\,406}{893\,918\,025}\right)x^5 + \mathcal{O}(x^6), \tag{31}$$

$$f_{21}^J(x;\nu) = 1 + \left(\frac{23\nu}{42} - \frac{59}{28}\right)x + \left(\frac{85\nu^2}{252} - \frac{269\nu}{126} - \frac{5}{9}\right)x^2 + \left(\frac{88\,404\,893}{11\,642\,400} - \frac{214}{105}\text{eulerlog}_1(x)\right)x^3 + \left(\frac{6313}{1470}\text{eulerlog}_1(x) - \frac{3\,399\,8136\,553}{4\,237\,833\,600}\right)x^4 + \mathcal{O}(x^5), \tag{32}$$

$$f_{33}(x;\nu) = 1 + \left(2\nu - \frac{7}{2}\right)x + \left(\frac{887\nu^2}{330} - \frac{3401\nu}{330} - \frac{443}{440}\right)x^2 + \left(\frac{147\,471\,561}{2\,802\,800} - \frac{78}{7}\text{eulerlog}_3(x)\right)x^3 + \left(39\text{eulerlog}_3(x) - \frac{53\,641\,811}{457\,600}\right)x^4 + \mathcal{O}(x^5), \tag{33}$$

$$f_{32}^J(x;\nu) = 1 + \frac{320\nu^2 - 1115\nu + 328}{90(3\nu - 1)}x + \frac{39544\nu^3 - 253\,768\nu^2 + 117\,215\nu - 20\,496}{11\,880(3\nu - 1)}x^2 + \left(\frac{110\,842\,222}{4\,729\,725} - \frac{104}{21}\text{eulerlog}_2(x)\right)x^3 + \mathcal{O}(x^4), \tag{34}$$

$$f_{31}(x;\nu) = 1 + \left(-\frac{2\nu}{3} - \frac{13}{6}\right)x + \left(-\frac{247\nu^2}{198} - \frac{371\nu}{198} + \frac{1273}{792}\right)x^2 + \left(\frac{400\,427\,563}{75\,675\,600} - \frac{26}{21}\text{eulerlog}_1(x)\right)x^3 + \left(\frac{169}{63}\text{eulerlog}_1(x) - \frac{12\,064\,573\,043}{1\,816\,214\,400}\right)x^4 + \mathcal{O}(x^5). \tag{35}$$

For convenience and readability, we have introduced the following "eulerlog" functions $\text{eulerlog}_m(x)$:

$$\text{eulerlog}_m(x) = \gamma_E + \log 2 + \tfrac{1}{2}\log x + \log m, \tag{36}$$

which explicitly reads, when $m = 1, 2, 3$,

$$\text{eulerlog}_1(x) = \gamma_E + \log 2 + \tfrac{1}{2}\log x, \tag{37}$$

$$\text{eulerlog}_2(x) = \gamma_E + 2\log 2 + \tfrac{1}{2}\log x, \tag{38}$$

$$\text{eulerlog}_3(x) = \gamma_E + \log 2 + \log 3 + \tfrac{1}{2}\log x, \tag{39}$$

where γ_E is Euler's constant, $\gamma_E = 0.577\,215\ldots$ and $\log(x)$ denotes, as everywhere else in this paper, the natural logarithm function.

D. Resumming the modulus factor $f_{\ell m}$

The decomposition of the total PN-correction factor $\hat{h}^{(\epsilon)}_{\ell m}$ into several factors is in itself a resummation procedure, which has already improved the convergence of the PN series one has to deal with: indeed, one can see that the coefficients entering increasing powers of x in the $f_{\ell m}$'s tend to be systematically smaller than the coefficients appearing in the usual PN expansion of $\hat{h}^{(\epsilon)}_{\ell m}$. The reason for this is essentially twofold: (i) the factorization of $T_{\ell m}$ has absorbed powers of $m\pi$, which contributed to making large coefficients in $\hat{h}^{(\epsilon)}_{\ell m}$, and (ii) the factorization of either $\hat{H}_{\rm eff}$ or $\hat{j}$ has (in the $\nu = 0$ case) removed the presence of an inverse square-root singularity located at $x = 1/3$, which caused the coefficient of x^n in any PN-expanded quantity to grow as 3^n as $n \to \infty$. To prevent some potential misunderstandings, let us emphasize that we are talking here about a singularity entering the analytic continuation (to larger values of x) of a mathematical function $h(x)$ defined (for small values of x) by considering the formal adiabatic circular limit. The point is that, in the $\nu \to 0$ limit, the radius of convergence and therefore the growth with n of the PN coefficients of $h(x)$ (Taylor expanded at $x = 0$), are linked to the singularity of the analytically continued $h(x)$, which is nearest to $x = 0$ in the complex x plane. In the $\nu \to 0$ case, the nearest singularity in the complex x plane comes from the source factor $\hat{H}_{\rm eff}(x)$ or $\hat{j}(x)$ in the waveform and is located at the light-ring $x_{\rm LR}(\nu = 0) = 1/3$. In the $\nu \neq 0$ case, the EOB formalism transforms the latter (inverse square-root) singularity into a more complicated ("branching") singularity, where $d\hat{H}_{\rm eff}/dx$ and $d\hat{j}/dx$ have inverse square-root singularities located at what is called [8,2,11,18,29] the (effective)[13] "EOB light ring," i.e., the (adiabatic) maximum of Ω, $x^{\rm adiab}_{\rm ELR}(\nu) \equiv (M\Omega^{\rm adiab}_{\rm max})^{2/3} \gtrsim 1/3$.

Despite this improvement, the resulting convergence of the usual Taylor-expanded $f_{\ell m}(x)$'s quoted above does not seem to be good enough, especially near or below the LSO, in view of the high accuracy needed to define gravitational wave templates. For this reason, Refs. [1,2] proposed to further resum the $f_{22}(x)$ function via a Padé (3, 2) approximant, $P^3_2\{f_{22}(x;\nu)\}$, so as to improve its behavior in the strong-field-fast-motion regime. Such a resummation gave an excellent agreement with numerically computed waveforms, near the end of the inspiral and during the beginning of the plunge, for different mass ratios [1,10,18]. Here, however, we wish to explore a new route for resumming $f_{\ell m}$, based on replacing $f_{\ell m}$ by its ℓ-th root, say

$$\rho_{\ell m}(x;\nu) = [f_{\ell m}(x;\nu)]^{1/\ell}. \tag{40}$$

Our basic motivation for replacing $f_{\ell m}$ by $\rho_{\ell m}$ is the following: the leading "Newtonian-level" contribution to the waveform $h^{(\epsilon)}_{\ell m}$ contains a factor $\omega^\ell r^\ell_{\rm harm} v^\epsilon$, where $r_{\rm harm}$ is the harmonic radial coordinate used in the MPM formalism [30,31]. When computing the PN expansion of this factor one has to insert the PN expansion of the (dimensionless) harmonic radial coordinate $r_{\rm harm}$, $r_{\rm harm} = x^{-1}(1 + c_1 x + \mathcal{O}(x^2))$, as a function of the gauge-independent frequency parameter x. The PN reexpansion of $[r_{\rm harm}(x)]^\ell$ then generates terms of the type $x^{-\ell}(1 + \ell c_1 x + \ldots)$. This is one (though not the only one) of the origins of 1PN corrections in $h_{\ell m}$ and $f_{\ell m}$ whose coefficients grow linearly with ℓ. As we shall see in detail below, these ℓ-growing terms are problematic for the accuracy of the PN expansions. Our replacement of $f_{\ell m}$ by $\rho_{\ell m}$ is a cure for this problem.

More explicitly, the investigation of 1PN corrections to GW amplitudes [12,30,31] has shown that, in the even-parity case (but see also Appendix A for the odd-parity case),

$$c_1^{f^{\rm even}_{\ell m}}(\nu) = -\ell\left(1 - \frac{\nu}{3}\right) + \frac{1}{2} + \frac{3}{2}\frac{c_{\ell+2}(\nu)}{c_\ell(\nu)} - \frac{b_\ell(\nu)}{c_\ell(\nu)} - \frac{c_{\ell+2}(\nu)}{c_\ell(\nu)}\frac{m^2(\ell+9)}{2(\ell+1)(2\ell+3)}, \tag{41}$$

where $c_\ell(\nu)$ is defined in Eq. (7) and, consistently with the notation of Appendix A,

$$b_\ell(\nu) \equiv X_2^\ell + (-)^\ell X_1^\ell. \tag{42}$$

As we shall see below, the ν dependence of $c_1^{f_{\ell m}}(\nu)$ is quite mild. For simplicity, let us focus on the $\nu = 0$ case, where the above result shows that the PN expansion of $f_{\ell m}$ starts as

$$f^{\rm even}_{\ell m}(x;0) = 1 - \ell x\left(1 - \frac{1}{\ell} + \frac{m^2(\ell+9)}{2\ell(\ell+1)(2\ell+3)}\right) + \mathcal{O}(x^2). \tag{43}$$

The crucial thing to note in this result is that as ℓ gets large (keeping in mind that $|m| \leq \ell$), the coefficient of x will be negative and will approximately range between $-5\ell/4$ and $-\ell$. This means that when $\ell \geq 6$ the 1PN correction in $f_{\ell m}$ would by itself make $f_{\ell m}(x)$ vanish before the ($\nu = 0$) LSO $x = 1/6$. For example, for the $\ell = m = 6$ mode, one

[13] Beware that this "effective EOB light ring" occurs for a circular-orbit radius slightly larger than the purely dynamical (circular) EOB light ring (where $H_{\rm eff}$ and $\mathcal{J}$ would formally become infinite).

has $f^{\rm 1PN}_{66}(x;0) = 1 - 6x(1 + 11/42) \approx 1 - 6x(1 + 0.26)$, which means a correction equal to -100% at $x = 1/7.57$ and larger than -100% at the LSO, namely, $f^{\rm 1PN}_{66}(1/6;0) \approx 1 - 1.26 = -0.26$. This is definitely incompatible with the numerical data we shall quote below. Similar results hold also for the odd-parity $f_{\ell m}$'s, especially in the case where we factorize the $\mathcal{J}$ source (which happens to have close similarities to the H-factored even-parity $f_{\ell m}$). Indeed, we have extended the result of Eq. (43) to the odd-parity case, i.e., we have computed, (using the comparable-mass 1PN results of Ref. [31]) the 1PN correction in $f_{\ell m}$ and $\rho_{\ell m}$. In the $\nu \to 0$ limit, we found that (see Appendix A for more details and for a discussion of the comparable-mass case)

$$f^J_{\ell m}(x;0) = 1 - \ell x \times \left(1 + \frac{1}{\ell} - \frac{2}{\ell^2} + \frac{m^2(\ell+4)}{2\ell(\ell+2)(2\ell+3)}\right) + \mathcal{O}(x^2), \tag{44}$$

which is structurally similar to the even-parity expression quoted above.

Let us now see how the replacement of $f_{\ell m}$ by the newly defined $\rho_{\ell m}$, Eq. (40), cures this problem of abnormally large 1PN corrections to the waveforms for large values of ℓ. Indeed, the Taylor expansion of $\rho_{\ell m}$ now starts as (say for simplicity in the $\nu = 0$, even-parity case)

$$\rho^{\rm even}_{\ell m}(x;0) = 1 - x\left(1 - \frac{1}{\ell} + \frac{m^2(\ell+9)}{2\ell(\ell+1)(2\ell+3)}\right) + \mathcal{O}(x^2). \tag{45}$$

Note that for large ℓ and arbitrary m the coefficient of x now approximately ranges between $-5/4$ and -1. We shall see below that the nice behavior of $\rho_{\ell m}$ expected from this 1PN estimate indeed holds for the exact $\rho_{\ell m}$, at least in the $\nu = 0$ case. In addition, the same structure is found in the odd-parity $\rho^J_{\ell m}$'s. In particular, from Eq. (44) above one finds

$$\rho^J_{\ell m}(x;0) = 1 - x \times \left(1 + \frac{1}{\ell} - \frac{2}{\ell^2} + \frac{m^2(\ell+4)}{2\ell(\ell+2)(2\ell+3)}\right) + \mathcal{O}(x^2), \tag{46}$$

where, for $\ell \gg 1$, the coefficient of x again approximately ranges between $-5/4$ and -1.

We have computed all the $\rho_{\ell m}$'s (both for the H and $\mathcal{J}$ choices) up to the highest available (ν dependent or not) PN accuracy. In the formulas for the $\rho_{\ell m}$'s given below we hybridize them by adding to the known ν-dependent coefficients $c_n^{\rho_{\ell m}}(\nu)$ in the Taylor expansion of $\rho_{\ell m}$'s,

$$\rho_{\ell m}(x;\nu) = 1 + c_1^{\rho_{\ell m}}(\nu)x + c_2^{\rho_{\ell m}}(\nu)x + c_3^{\rho_{\ell m}}(\log(x);\nu)x^3 + \ldots, \tag{47}$$

the $\nu = 0$ value of the higher-order coefficients $c_{n'}^{\rho_{\ell m}}(\nu = 0)$. Beware that this definition of an hybrid $\rho_{\ell m}$ is *not* equivalent to that displayed in Eqs. (31)–(35) above of an analogous hybrid $f_{\ell m}$ (nor is it equivalent to a straightforward hybridization of $h_{\ell m}$). The primary hybridization procedure that we advocate (and use) in this paper is the one based on $\rho_{\ell m}$ (i.e., replacing $c_{n'}^{\rho_{\ell m}}(\nu)$ by $c_{n'}^{\rho_{\ell m}}(0)$ when n' is beyond the maximal ν-dependent PN knowledge). The 1PN-accurate $\rho_{\ell m}$'s for $\ell + m$ even and—thanks to the new results for $h_{\ell m}$ for $\ell + m$ odd in Appendix A—also for $\ell + m$ odd are explicitly known for all ℓ. For the 1PN coefficient of the $\rho_{\ell m}$'s we explicitly have

$$c_1^{\rho^{\rm even}_{\ell m}}(\nu) = -\left(1 - \frac{\nu}{3}\right) + \frac{1}{2\ell} + \frac{3}{2\ell}\frac{c_{\ell+2}(\nu)}{c_\ell(\nu)} - \frac{1}{\ell}\frac{b_\ell(\nu)}{c_\ell(\nu)} - \frac{m^2(\ell+9)}{2\ell(\ell+1)(2\ell+3)}\frac{c_{\ell+2}(\nu)}{c_\ell(\nu)}, \tag{48}$$

$$c_1^{\rho^J_{\ell m}}(\nu) = -\left(1 - \frac{\nu}{3}\right) - \frac{1}{2\ell}\left(5 - \frac{\nu}{3}\right) - \frac{\nu}{2\ell^2} + \frac{2\ell+3}{2\ell^2}\frac{b_{\ell+1}(\nu)}{c_{\ell+1}(\nu)} + 2\nu\frac{\ell+1}{\ell^2}\frac{b_{\ell-1}(\nu)}{c_{\ell+1}(\nu)} + \frac{1}{2}\frac{\ell+1}{\ell^2}\frac{c_{\ell+3}(\nu)}{c_{\ell+1}(\nu)} - \frac{m^2(\ell+4)}{2\ell(\ell+2)(2\ell+3)}\frac{c_{\ell+3}(\nu)}{c_{\ell+1}(\nu)}. \tag{49}$$

For definiteness, we give in Appendix B the complete results, for $\rho_{\ell m}$ (even parity) and $\rho^J_{\ell m}$ (odd parity), up to $\ell = 8$ included. Here, for illustrative purposes, we quote only some of the lowest multipole results up to $\ell = 3$ included.

$$\rho_{22}(x;\nu) = 1 + \left(\frac{55\nu}{84} - \frac{43}{42}\right)x + \left(\frac{19\,583\nu^2}{42\,336} - \frac{33\,025\nu}{21\,168} - \frac{20\,555}{10\,584}\right)x^2 + \left(\frac{1\,062\,0745\nu^3}{39\,118\,464} - \frac{6\,292\,061\nu^2}{3\,259\,872} + \frac{41\pi^2\nu}{192} - \frac{48\,993\,925\nu}{9\,779\,616} - \frac{428}{105}\,\mathrm{eulerlog}_2(x) + \frac{1\,556\,919\,113}{122\,245\,200}\right)x^3 + \left(\frac{9202}{2205}\,\mathrm{eulerlog}_2(x) - \frac{387\,216\,563\,023}{160\,190\,110\,080}\right)x^4 + \left(\frac{439\,877}{55\,566}\,\mathrm{eulerlog}_2(x) - \frac{16\,094\,530\,514\,677}{533\,967\,033\,600}\right)x^5 + \mathcal{O}(x^6), \tag{50}$$

$$\rho^J_{21}(x;\nu) = 1 + \left(\frac{23\nu}{84} - \frac{59}{56}\right)x + \left(\frac{617\nu^2}{4704} - \frac{10\,993\nu}{14\,112} - \frac{47\,009}{56\,448}\right)x^2 + \left(\frac{7\,613\,184\,941}{2\,607\,897\,600} - \frac{107}{105}\mathrm{eulerlog}_1(x)\right)x^3 + \left(\frac{6313}{5880}\mathrm{eulerlog}_1(x) - \frac{1\,168\,617\,463\,883}{911\,303\,737\,344}\right)x^4 + \mathcal{O}(x^5), \tag{51}$$

$$\rho_{33}(x;\nu) = 1 + \left(\frac{2\nu}{3} - \frac{7}{6}\right)x + \left(\frac{149\nu^2}{330} - \frac{1861\nu}{990} - \frac{6719}{3960}\right)x^2 + \left(\frac{3\,203\,101\,567}{227\,026\,800} - \frac{26}{7}\mathrm{eulerlog}_3(x)\right)x^3 + \left(\frac{13}{3}\mathrm{eulerlog}_3(x) - \frac{57\,566\,572\,157}{8\,562\,153\,600}\right)x^4 + \mathcal{O}(x^5), \tag{52}$$

$$\rho^J_{32}(x;\nu) = 1 + \frac{320\nu^2 - 1115\nu + 328}{270(3\nu - 1)}x + \frac{3\,085\,640\nu^4 - 20\,338\,960\nu^3 - 4\,725\,605\nu^2 + 8\,050\,045\nu - 1\,444\,528}{1\,603\,800(1 - 3\nu)^2}x^2 + \left(\frac{5\,849\,948\,554}{940\,355\,325} - \frac{104}{63}\mathrm{eulerlog}_2(x)\right)x^3 + \mathcal{O}(x^4), \tag{53}$$

$$\rho_{31}(x;\nu) = 1 + \left(-\frac{2\nu}{9} - \frac{13}{18}\right)x + \left(-\frac{829\nu^2}{1782} - \frac{1685\nu}{1782} + \frac{101}{7128}\right)x^2 + \left(\frac{11\,706\,720\,301}{6\,129\,723\,600} - \frac{26}{63}\mathrm{eulerlog}_1(x)\right)x^3 + \left(\frac{169}{567}\mathrm{eulerlog}_1(x) + \frac{2\,606\,097\,992\,581}{4\,854\,741\,091\,200}\right)x^4 + \mathcal{O}(x^5). \tag{54}$$

III. RESULTS FOR THE EXTREME-MASS-RATIO CASE ($\nu = 0$)

A. Extracting the $\rho^{\mathrm{Exact}}_{\ell m}$ multipoles from black-hole perturbation numerical data

To test our new resummation procedure based on the $\rho_{\ell m}$'s we shall compare the analytical results defined by our multiplicative decomposition Eq. (8) to the exact results obtained by numerical analysis of black-hole perturbation theory. For most of the comparisons discussed below we will rely on data kindly provided by E. Berti, who computed the multipolar decomposition of the GW flux from stable circular orbits above the LSO with a frequency-domain code, which solves numerically the Teukolsky equation with a point-particle source. (see, for example, Ref. [17] and references therein). In addition, we have complemented Fig. 5 by computing the quadrupolar GW energy flux F_{22} from a sample of unstable circular orbits with radius between $6M$ and $3.1M$.

The result of the numerical computation is expressed in terms of the multipolar pieces $F_{\ell m}$ of the total exact flux, Eq. (2). We shall only consider multipoles up to $\ell = 6$ included. The exact $\nu \to 0$ version of our new quantities $\rho_{\ell m}(x;\nu)$'s are then obtained from the ratio of the exact partial fluxes $F^{\mathrm{Exact}}_{\ell m}$ to their Newtonian counterparts $F^{\mathrm{Newton}}_{\ell m}$ as

$$\rho^{\mathrm{Exact},(\epsilon)}_{\ell m}(x;0) = \left\{\frac{\sqrt{F^{\mathrm{Exact}}_{\ell m}/F^{\mathrm{Newton}}_{\ell m}}}{|T_{\ell m}|\hat{S}^{(\epsilon)}_{\mathrm{eff}}}\right\}^{1/\ell}, \tag{55}$$

where, for $\nu = 0$, we explicitly have

$$\hat{S}^{(0)}_{\mathrm{eff}}(x) = \frac{1 - 2x}{\sqrt{1 - 3x}}, \tag{56}$$

and either

$$\hat{S}^{(1,H)}_{\mathrm{eff}}(x) = \frac{1 - 2x}{\sqrt{1 - 3x}}, \tag{57}$$

or

$$\hat{S}^{(1,J)}_{\mathrm{eff}}(x) = \frac{1}{\sqrt{1 - 3x}}. \tag{58}$$

Still in the $\nu \to 0$ limit, we have $H_{\mathrm{real}} \to M$, and, from well-known properties of the Γ function, the square modulus of the tail factor $T_{\ell m}$ reads

$$|T_{\ell m}|^2 = \frac{1}{(\ell!)^2}\frac{4\pi\hat{\hat{k}}}{1 - e^{-4\pi\hat{\hat{k}}}}\prod_{s=1}^{\ell}[s^2 + (2\hat{\hat{k}})^2], \tag{59}$$

where now $\hat{\hat{k}} = mM\Omega = mx^{3/2} = mv^3$.

B. Finding structure in the $\rho^{\mathrm{Exact}}_{\ell m}$ multipoles extracted from numerical data

Let us first consider the properties of the exact $\rho_{\ell m}$'s. In the odd-parity case we shall focus here on the $\mathcal{J}$-normalized quantity $\rho^J_{\ell m}$. We shall see that the $\rho_{\ell m}$'s convey interesting information about the x dependence of the multipolar GW amplitudes. Figure 3 exhibits the numerical $\rho_{\ell m}$ functions for $\ell \le 6$, versus $x = (M\Omega)^{2/3}$ (where we recall that Ω denotes the orbital frequency) up to the $\nu = 0$ LSO, $x = 1/6$. Each panel of the figure displays, for each given $2 \le \ell \le 6$, the partial $\rho_{\ell m}$'s for the various possible m's, $1 \le m \le \ell$ (we do not plot the

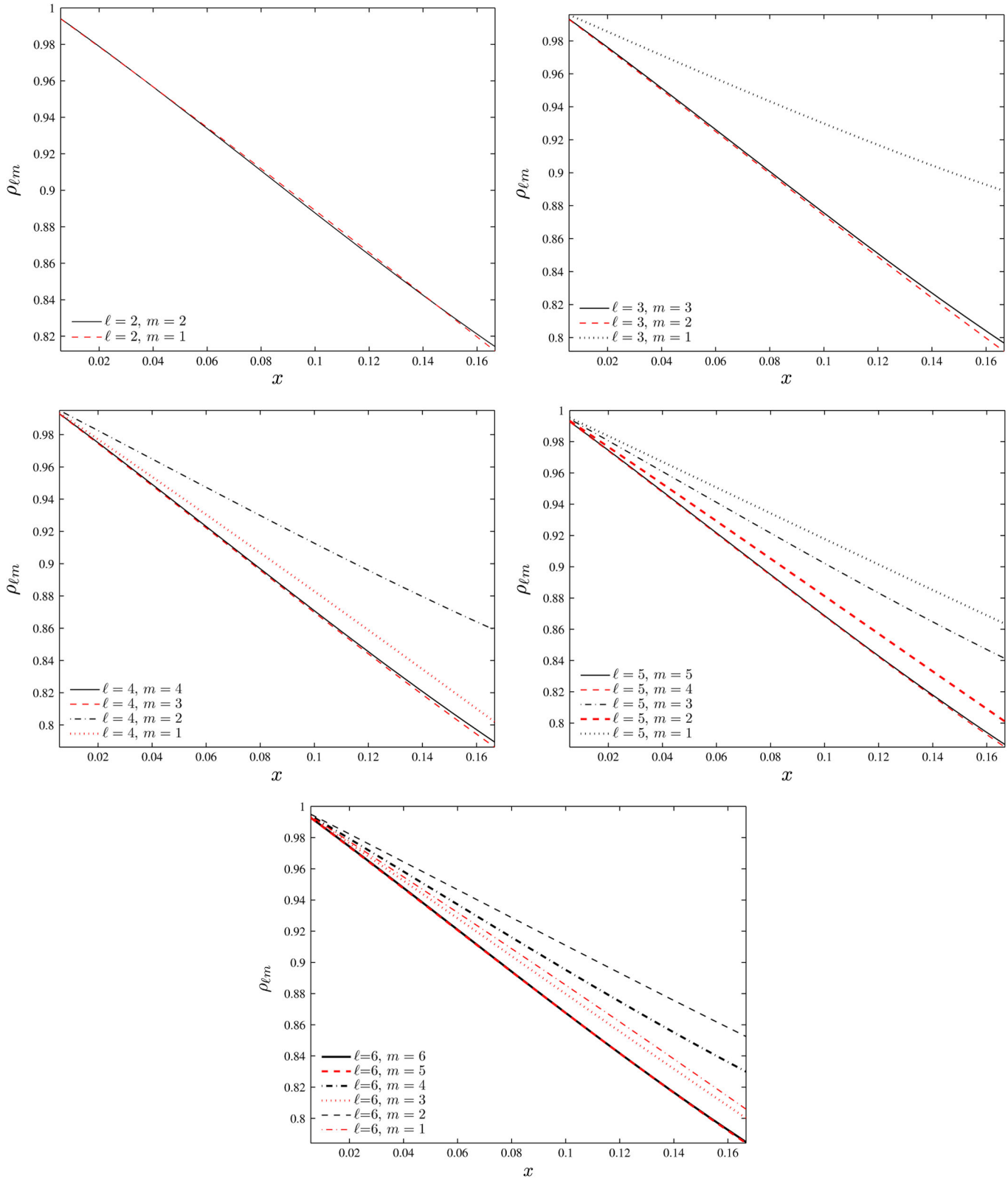

FIG. 3 (color online). Extreme-mass-ratio limit ($\nu = 0$). The exact functions $\rho_{\ell m}(x)$ for $0 < x < 1/6$ extracted from E. Berti's numerical fluxes. Multipoles up to $\ell = 6$ are considered. Each panel corresponds to one value of ℓ and shows the even-parity partial amplitudes (black online) together with the *J-normalized* odd-parity ones (red online).

negative m's since they correspond to the same value of $\rho_{\ell m}$). The even-parity ($\ell + m$ even, black online) and odd-parity ($\ell + m$ odd, red online) modes are shown together for comparison.

Figure 3 displays the following noticeable facts: (i) to a good approximation, all the $\rho_{\ell m}(x)$ are *straight lines*[14] [see below]; (ii) for each value of ℓ, the (negative) slopes of the dominant $m = \ell$ (even-parity), and subdominant $m = \ell - 1$ (odd-parity) multipole modes are very close to each other; and these slopes become closer and closer as the value of ℓ increases (note, in particular, that for $\ell = 6$ $\rho_{66}(x)$ and $\rho_{65}(x)$ are practically coincident); (iii) for a given value of ℓ, *and a given parity* (even or odd), the absolute value of the (negative) slope decreases monotonically as $|m|$ decreases. This "order" in the exact data can be analytically understood.

The property (i) means that the *1PN correction is already capturing most of the physical information*, which might turn out to be a useful fact to know (see below). We illustrate this result in Fig. 4, which focuses on the quadrupolar ($\ell = 2$) partial waves, and exhibits the exact ρ_{22} and ρ^J_{21} (solid and dashed lines) together with their 1PN approximations (dotted lines). Note, for instance, that the difference between the 1PN accurate, $\rho^{\rm 1PN}_{22}$, that we shall denote[15] $T_1[\rho_{22}] \equiv \rho^{\rm 1PN}_{22} = 1 + c^{\rho_{\ell m}}_1 x$, and the exact one $\rho^{\rm Exact}_{22}$ is equal, at the LSO, to $\rho^{\rm 1PN}_{22} - \rho^{\rm Exact}_{22} = 0.8294 - 0.8143 = 0.0151$, which is only 1.9% of the exact result 0.8143. The other multipoles exhibit a similar agreement between the exact $\rho_{\ell m}$ and their analytical 1PN representations. To understand analytically what underlies this agreement, let us consider the $\ell = m = 2$ case. Numerically, from Eq. (50) we have, near the LSO [for simplicity, we replace the $\log(x)$ terms present in the coefficients by their numerical values at $x = 1/6$]

$$\begin{aligned}\rho_{22}(x;0) &\approx 1 - 1.024x - 1.942x^2 + 8.384x^3 + 2.038x^4 \\ &\quad - 21.690x^5 \\ &\approx 1 - 0.171(6x) - 0.054(6x)^2 + 0.039(6x)^3 \\ &\quad + 0.0016(6x)^4 - 0.0028(6x)^5. \end{aligned} \tag{60}$$

We see that the successive coefficients of the PN expansion of ρ_{22} are such that, even at the LSO, the magnitudes of the PN corrections beyond the 1PN one are rather small. They are significantly smaller than the corresponding terms in the usual PN expansion of the total flux. For instance, by contrast to the coefficient -21.69, which enters the 5PN correction in ρ_{22}, let us recall that the coefficient [including the $\log(x)$ estimated at the LSO] of the 5PN correction in the usual PN-expanded flux is ≈ -1321.402 (see, e.g., [6]). Note that the latter 5PN contribution to the PN-expanded flux considered at the LSO is $-1321.40/6^5 \approx -0.17$, which is as large as the 1PN contribution to ρ_{22} and about 60 times larger than the corresponding 5PN correction to ρ_{22}. In addition, as the signs in Eq. (60) fluctuate, there are compensations between the higher PN contributions, as it will be clear from further results presented below.

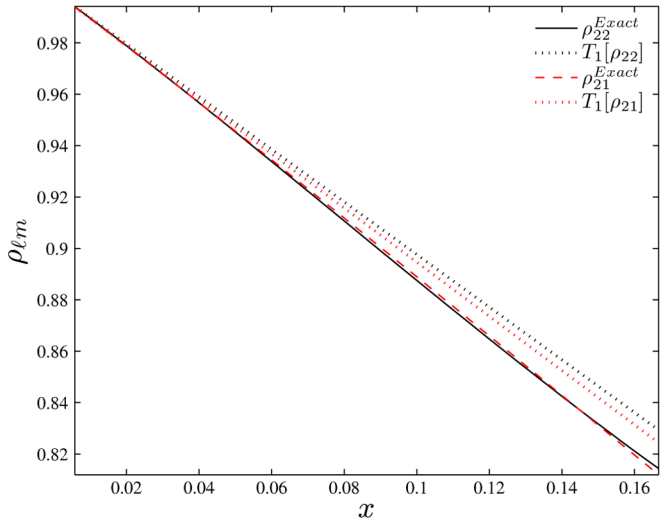

FIG. 4 (color online). Extreme-mass-ratio limit ($\nu = 0$). Comparison between the exact leading and subleading quadrupolar amplitudes ρ_{22} and ρ^J_{21} and the corresponding 1PN-accurate analytical ones.

Property (ii) can be analytically understood by means of the 1PN-accurate closed formulas, Eqs. (45) and (46). Indeed, it is easily checked that the difference between the coefficients of x Eq. (45) for $m = \ell$ and Eq. (46) for $m = \ell - 1$ is of order $\mathcal{O}(1/\ell^2)$ when ℓ gets large.

Finally, property (iii) is understood by noting that the coefficients of x in Eqs. (45) and (46) have the structure $-(a(\ell) + m^2 b(\ell))$, where $a(\ell)$ and $b(\ell)$ are positive.

C. Comparing Taylor and Padé approximants of ρ_{22}

Let us now compare and contrast the convergence of various PN approximants toward the exact (numerical) ρ_{22}. We first focus on the values of various approximants to $\rho_{22}(x)$ at the LSO, i.e., at $x_{\rm LSO} = 1/6$ or actually the last point in the numerical data computed by E. Berti, $x_{\rm last} = 1/6.00\,001$. At the point $x = x_{\rm last}$ the numerical value of the Newton-normalized $\ell = m = 2$ partial flux is $\hat{F}_{22} \equiv F_{22}/F^N_{22} = 0.8\,927\,266\,028$. This corresponds to $\rho^{\rm Exact}_{22}(x_{\rm last}) = 0.8\,143\,372\,247$. In Table II we compare this value to several PN-based approximants: both Taylor approximants, from 1PN to 5PN ($T_1[\rho_{22}]$ to $T_5[\rho_{22}]$) and several of the "around the diagonal" 5PN-accurate Padé approximants, namely, $P^4_1\{T_5[\rho_{22}]\}$, $P^1_4\{T_5[\rho_{22}]\}$,

[14] In the odd-parity case, $\ell + m$ odd, this quasilinear behavior up to the LSO, is particularly clear for the functions $\rho^J_{\ell m}(x)$'s, making us consider $\rho^J_{\ell m}$ as our best default choice. By contrast, the H-normalized functions $\rho^H_{\ell m}(x)$ have a more ℓ-dependent shape that the reader can figure out by noting the link between them: $\rho^H_{\ell m} = \rho^J_{\ell m}/(1-2x)^{1/\ell}$.

[15] Here and in the following we shall denote the truncated n-PN-accurate expansion of any function $f(x)$ as $T_n[f(x)] \equiv f_0 + f_1 x + \ldots + f_n x^n$.

TABLE II. Closeness of various resummed approximants to ρ_{22} at the LSO, $x_{\rm LSO} = 1/6$, or actually $x_{\rm last} = 1/6.00\,001$. The right-most column lists the difference $\Delta\rho_{22}$ between the resummed approximant and the exact value at $x = x_{\rm last}$.

Approximant	$\rho_{22}(x_{\rm last})$	$\Delta\rho_{22}(x_{\rm last})$
$\rho_{22}^{\rm Exact}$	0.8 143 372 247	0
$T_1[\rho_{22}]$	0.8 293 653 638	0.0 150 281 391
$T_2[\rho_{22}]$	0.7 754 188 106	−0.038 9184 141
$T_3[\rho_{22}]$	0.8 142 342 355	−0.0 001 029 892
$T_4[\rho_{22}]$	0.8 158 069 452	0.0 014 697 205
$T_5[\rho_{22}]$	0.8 130 176 477	−0.0 013 195 770
$P_1^4\{T_5[\rho_{22}]\}$	0.8 148 012 716	0.0 004 640 469
$P_4^1\{T_5[\rho_{22}]\}$	0.8 146 954 164	0.0 003 581 917
$P_2^3\{T_5[\rho_{22}]\}$	0.8 132 320 684	−0.0 011 051 563
$P_3^2\{T_5[\rho_{22}]\}$	0.8 146 954 104	0.0 003 581 857

$P_2^3\{T_5[\rho_{22}]\}$, and $P_3^2\{T_5[\rho_{22}]\}$. Note how the sequence of Taylor approximants to ρ_{22} nicely approaches the exact value, especially starting with the 3PN approximation. Probably by accident, the Taylor 3PN approximant, $T_3[\rho_{22}]$, happens to be closer to the exact value than the higher-order approximants T_4 and T_5. Besides this accidental closeness of T_3, the important thing to note is the very small dispersion (within $\pm 1.8 \times 10^{-3}$) of T_3, T_4, and T_5 around the correct value. This excellent behavior of the Taylor approximants of ρ_{22} should be contrasted with the much worse behavior of the standard Taylor approximants either of the flux or of the waveforms (see, for example, Fig. 1 in Ref. [5], Fig. 3 in Ref. [6] and Fig. 6 below, where we directly compare the usual Taylor approximants to the waveform to our new $\rho_{\ell m}$-based approximants). Note that when considering "Taylor approximants to ρ_{22}" we are actually speaking of a specifically *resummed* approximant to the waveform $\hat{h}_{22}$. This approximant has the factorized form of Eq. (8), and is made of the product of several resummed constituents. Even the last factor f_{22} of this product is not used in Taylor-expanded form (which would be $T_5[f_{22}]$), but in the minimally resummed way $f_{22}^{\rm Resummed} = (T_5[\rho_{22}])^2$.

We have also explored several ways of further resumming ρ_{22}, i.e., of replacing its PN-expanded form $T_5[\rho_{22}]$ by various non-Taylor approximants. In view of the good closeness of the 1PN approximation to ρ_{22} to the exact result we explored, in particular, some "factorized" approximants (similar to those considered for the $A(u)$ function in Ref. [32]) of the type $\rho_{22}(x) = (1 + c_1^{\rho_{22}} x)\bar{\rho}_{22}(x)$. We will not show our results for these approximants here. Instead, let us discuss the use of Padé approximants for representing $T_5[\rho_{22}]$ as a rational function[16] of x. As an example, we present in Table II the values of $\rho_{22}(x_{\rm last})$ predicted by using the four "around the diagonal" 5PN accurate Padé approximants, namely, $P_1^4\{T_5[\rho_{22}]\}$, $P_4^1\{T_5[\rho_{22}]\}$, $P_2^3\{T_5[\rho_{22}]\}$, and $P_3^2\{T_5[\rho_{22}]\}$. The important thing to note is that all these approximants are both consistently clustered among themselves, as well as closely centered around the correct numerical value (within $\pm 1.3 \times 10^{-3}$). Note also that, apart from T_3, all the Padé approximants are closer to the exact value than the T_4 and T_5. (Though the *a priori* less-accurate T_3 approximant happens to be closer to the exact value than all other approximants, we consider that this is coincidental because the subsequent Taylor approximants T_4 and T_5 do not exhibit such a close proximity.)

We display in Fig. 5, the various 5PN-accurate approximants discussed above (together with the 1PN-accurate $T_1[\rho_{22}]$ for comparison) to $\rho_{22}(x)$ over the *larger interval* $0 \le x \le x_{\rm LR}$, where $x_{\rm LR} = 1/3$ is the value of the frequency parameter x at the $(\nu = 0)$ "light ring." Note that, while all the 5PN approximants stay very close to each other (and to the exact numerical value, red online) up to the LSO, they start diverging from each other when $x \gtrsim 0.2$. This motivated us to extend the numerical data of E. Berti beyond the LSO, i.e., to consider the GW flux emitted by unstable circular orbits of Schwarzschild radii $3GM \le R \equiv GMr \le 6GM$, corresponding to $1/6 \le x \le 1/3$. See Table III for results obtained for such a sample of sub-LSO orbits (they also appear in Fig. 5 as empty circles). These numbers have been computed with the time-domain code described in Ref. [33]. A resolution of $\Delta r_* = 0.01$

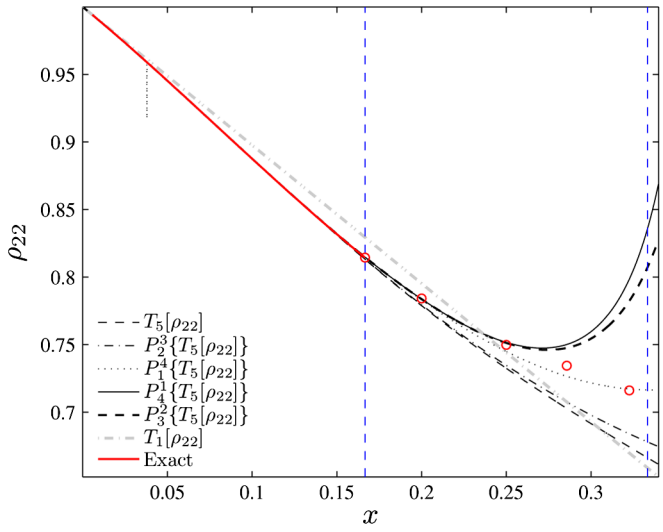

FIG. 5 (color online). Extreme-mass-ratio limit $(\nu = 0)$. Resummation of the function $\rho_{22}(x)$ on the interval $0 \le x \le 1/3$: comparison between various Taylor and Padé approximants and the exact function obtained from (both frequency-domain and time-domain) numerical calculations. The time-domain data points (see Table III) are indicated as empty circles.

[16] As in Ref. [2] we consider in this work the logarithmic terms (of the type $\text{eulerlog}_m(x)$ in Eqs. (50)–(54)) as part of the coefficients when Padéing $\rho_{\ell m}(x)$

TABLE III. Newton-normalized energy flux, and partial amplitudes f_{22} and ρ_{22}, for a sample of unstable circular orbits computed via the time-domain code of Ref. [33]. These values of ρ_{22} are represented as empty circles in Fig. 5. The case $r = 6$ is shown here only for comparison with frequency-domain-based results.

r	x	$\hat{F}_{22}^{\rm time}$	$f_{22}^{\rm time}$	$\rho_{22}^{\rm time}$
6	0.1666	0.897	0.665	0.815
5	0.2000	0.995	0.615	0.784
4	0.2500	1.378	0.562	0.750
3.5	0.2857	2.202	0.539	0.734
3.1	0.3226	6.665	0.513	0.716

was used. To test the accuracy of our numerical procedure we computed the energy flux $\hat{F}_{22}$ at $r = 6$ and compared it with the value obtained via Berti's frequency-domain code (at the very close value $r = 6.00\,001$). We obtained $\hat{F}_{22}^{\rm time} = 0.897\,342$ to be contrasted with $\hat{F}_{22}^{\rm freq} = 0.892726$, which yields a fractional difference $\Delta\hat{F}/\hat{F}^{\rm freq} \approx 0.005$. This gives an indication of the accuracy of our time-domain results, though we expect, for various numerical reasons, that the accuracy degrades as r gets below 4.

We do not wish to give too much weight to the indication given by our sub-LSO results on the behavior of the function $\rho_{22}(x)$ below the LSO. Indeed, on the one hand, the GW flux along sub-LSO circular orbits does represent the analytic continuation of the function $F(x)$ yielding the GW flux along (stable) super-LSO circular orbits. As such, the empty circles in Fig. 5 do provide correct mathematical information about the analytical continuation of the function $\rho_{22}(x)$ that we are trying to best approximate. On the other hand, we are evidently aware that the real dynamics of the "plunge" strongly deviates from the sequence of unstable circular orbits below the LSO and that the GW flux emitted by a plunging test mass (or effective source) will not be correctly represented by this mathematical continuation of $F(x)$. However, we expect, especially on the basis of the EOB formalism, which has shown that plunging orbits remain approximately quasicircular, that, in view of the present approach where we decompose the GW amplitude into several different factors having different physical origin, the mathematical continuation of the ρ_{22} part is likely to continue to capture important aspects of the nonlinear relativistic corrections to the waveform [note that we have in mind using our factorized waveform Eq. (8) along the EOB quasicircular plunge together with the correct instantaneous source $\hat{S}_{\rm eff}^{(\epsilon)}$ and tail corrections $T_{\ell m}$]. However, we are also aware that some aspects of the EOB plunge do physically differ, near the end of the plunge, in a relevant way from the physics included in the mathematical continuation of $\rho_{22}(x)$, namely, the fact that the ratio $(m\Omega)^2/V_\ell(r)$ (where $V_\ell(r)$ is the Zerilli potential) stays always small along the real plunge, while it increases more along unstable circular orbits and ends up reaching values of order unity. In other words the part of $\rho_{22}(x)$, which takes into account the filtering of $V_\ell(r)$, will be different in the two cases for orbits near the light ring. However, with due reserve we think that the first three empty circles on Fig. 5 do provide a guideline for selecting among the various diverging PN approximants the ones that are likely to provide, within the EOB formalism, a good zeroth-order approximation to the wave amplitude emitted by real plunging orbits. But, we expect that it will be necessary to correct such a zeroth-order quasicircular wave amplitude by non-quasi-circular corrections of the type that has already been found necessary in Refs. [1,18] to obtain a close agreement between EOB waveforms and numerical waveforms.

If we use such a guideline, Fig. 5 suggests that the best continuations of $\rho_{22}(x)$ below the LSO are given by the three particular Padé approximants, P_4^1, P_1^4, and P_3^2. However, as P_1^4 develops a spurious pole (which is barely visible on the left upper corner of the figure because it is very localized) at $x \approx 0.038$ we will discard it. By contrast, the other two are robust against the presence of spurious poles in the useful regime $x \lesssim 1/3$ (although they develop poles for higher values of x, namely, below the formal "event horizon" value $x = 1/2$). In the following, we shall choose P_3^2 as our current best-bet approximant to the ρ_{22} function (notably because this is the natural near-diagonal default Padé approximant). Note finally, in Fig. 5, how the simple 1PN-accurate Taylor approximant of $\rho_{22}(x)$ succeeds in providing a reasonably good representation of $\rho_{22}^{\rm Exact}(x)$ over a very large range of x values.

D. Comparing resummed waveforms to Taylor-expanded and exact ones

Up to now, we focussed on the convergence of various PN-based approximants toward the numerically determined value of the fourth technical building block ρ_{22} entering the dominant quadrupolar wave.

In this subsection we shall investigate instead the convergence of various possible PN-based approximants toward the more physically relevant Newton-normalized GW amplitudes $\hat{h}_{\ell m}$. On the one hand, we shall consider not only the dominant $\ell = m = 2$ wave, but also a selection of subdominant partial waves. On the other hand, we shall consider other PN-based approximants than those considered above. In particular, we shall compare and contrast the exact moduli $|\hat{h}_{\ell m}|$ both with standard high-accuracy Taylor-expanded waveforms ($|\hat{h}_{\ell m}| = 1 + c_1 x + c_{1.5}x^{3/2} + c_2 x^2 + \ldots$), and with our new "resummed with Taylor [ρ]" waveforms ($|\hat{h}_{\ell m}| = \hat{S}_{\rm eff}|T_{\ell m}|\rho_{\ell m}^{\ell}$ with $\rho_{\ell m} = 1 + c_1' x + c_2' x^2 + c_3' x^3 + \ldots$). We shall also analyze the performance of our new "resummed with Padé[ρ]" waveforms ($|\hat{h}_{\ell m}| = \hat{S}_{\rm eff}|T_{\ell m}|\rho_{\ell m}^{\ell}$ with $\rho_{\ell m} = P_p^q[1 + c_1' x + c_2' x^2 + c_3' x^3 + \ldots]$), at least for the $\ell = m = 2$ dominant

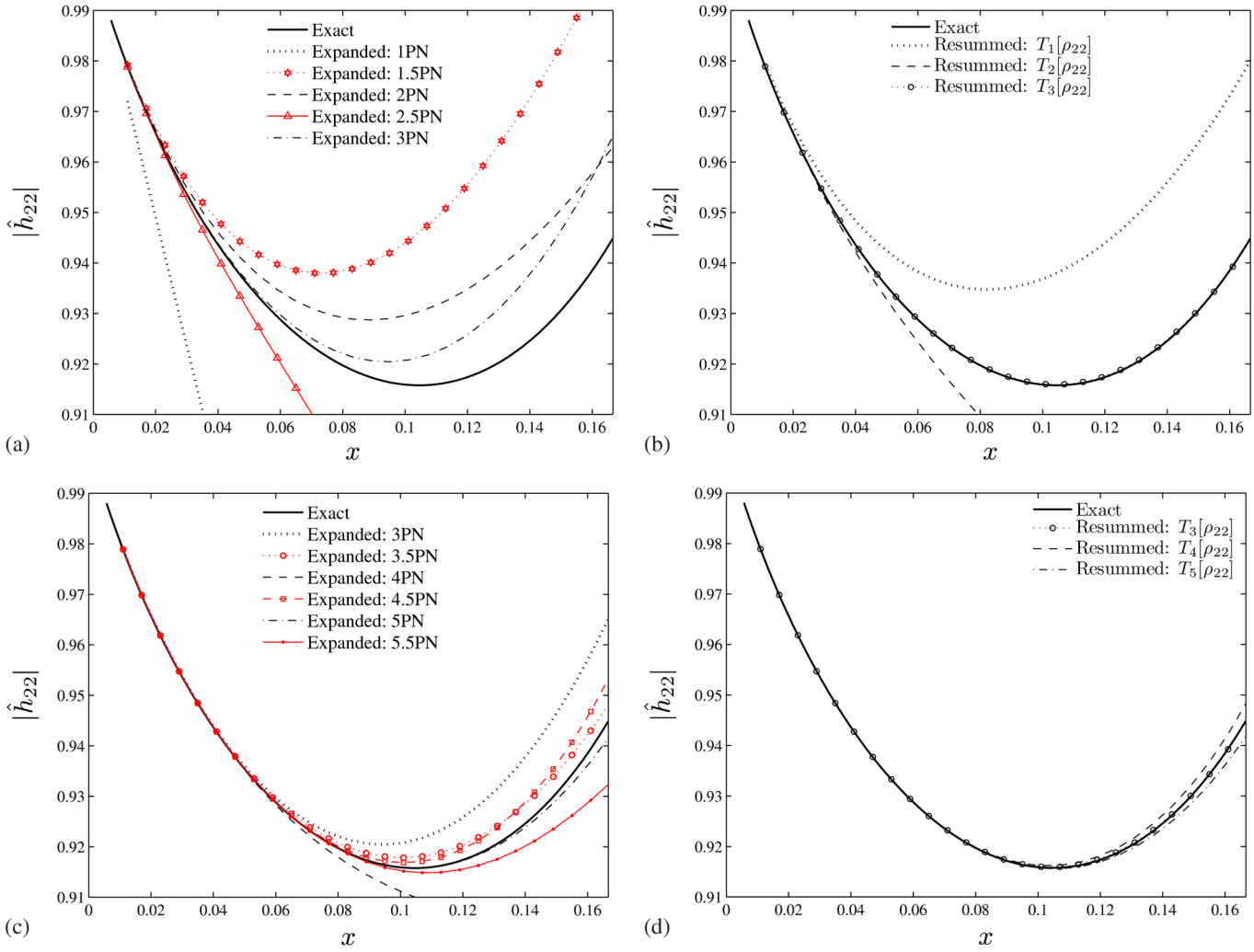

FIG. 6 (color online). Extreme-mass-ratio limit ($\nu = 0$): Various representations of the $|\hat{h}_{22}|$ waveform modulus. Left panels: standard PN-expanded amplitudes. Right panels: Various resummed amplitudes. See text for details.

mode.[17] For definiteness, we discuss here only, besides the dominant even-parity quadrupole mode $|\hat{h}_{22}|$, the first subdominant odd-parity mode $|\hat{h}_{21}|$, as well as the dominant $\ell = 4$ mode $|\hat{h}_{44}|$.

Figure 6 focusses on $|\hat{h}_{22}|$. The left panels, (a) and (c), display the standard Taylor-expanded $|\hat{h}_{22}| = 1 + c_1 x + c_{1.5} x^{3/2} + c_2 x^2 + \ldots$. More precisely, panel (a) considers the standard Taylor-expanded amplitudes up to 3PN accuracy included, while panel (c) displays the standard Taylor-expanded amplitudes from 3PN to 5.5PN accuracy. By contrast, the right panels, (b) and (d), display our new "resummed with Taylor [ρ]" approximants: panel (b) exhibits the 1PN, 2PN and 3PN approximants, while panel (d) contrasts the 3PN, 4PN and 5PN approximants.[18] Consistently with previous studies [5,6] (done at the level of the flux) there is evidently more scatter in the standard Taylor-expanded amplitudes than in the resummed ones. In particular, note that the standard 1PN-accurate Taylor approximant gives a grossly inaccurate representation of $\hat{h}_{22}$ as soon as $x \gtrsim 0.05$ (building up to -40% at the LSO), while our new-resummed $T_1[\rho_{22}]$-based waveform not only captures the qualitative behavior of the exact waveform, but also reproduces it quantitatively within $\sim 4\%$ even at the LSO. On the other hand, for 3PN and higher accuracies the resummed waveforms exhibit a very close

[17] In view of the remarkable agreement, displayed in panel (d) of Fig. 1, between the exact total flux $\hat{F}(x)$ and the results obtained by using only "resummed with Taylor [ρ]" approximants, we will not discuss here the probable improvements that a further Padéing of the subdominant $\rho_{\ell m}$'s might bring in.

[18] Note that because our tail factor (together with $e^{i\delta_{\ell m}}$) has conveniently resummed all the half-integer powers of x, the left panels have to include half-integer PN approximants, while the right panels have only integer-power approximants.

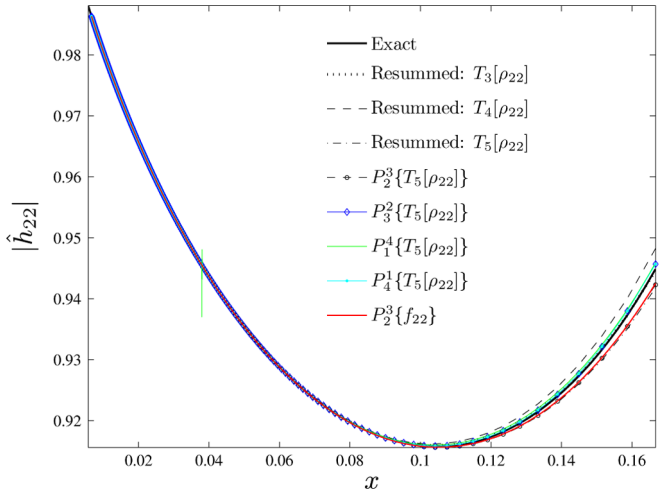

FIG. 7 (color online). Extreme-mass-ratio limit ($\nu = 0$). Resummation of the $|\hat{h}_{22}|$ waveform modulus: contrasting "resummed with Taylor $[\rho]$" approximants with some 5PN accurate "resummed with Padé $[\rho]$" approximants. See text for definitions and explanations.

agreement (within $\pm 1 \times 10^{-3}$) with the exact one.[19] In previous work [1,2], we had proposed to resum $\hat{h}_{22}$ by Padé (P_2^3) approximating $f_{22} = (\rho_{22})^2$ instead of ρ_{22}. For completeness, we compare in Fig. 7 our previous best proposal to the cluster of our current best proposals (based on various Taylor and Padé approximants of ρ_{22}). In first approximation, this figure shows a rather close agreement between all these approximants. In second approximation, one can note that some of our new approximants, namely, P_3^2, P_4^1, and P_1^4, are closer to the exact numerical results. From the pragmatic point of view, our current best-bet approximants are therefore our two new, pole-free, Padé approximants based on $P_3^2\{T_5[\rho_{22}]\}$ and $P_4^1\{T_5[\rho_{22}]\}$. We have a slight preference for $P_3^2\{T_5[\rho_{22}]\}$, which is the normal subdiagonal Padé (admitting a simple continuous fraction representation) and which was close to the sub-LSO numerical results (see Fig. 5).

Figure 8 exhibits the results for $|\hat{h}_{21}|$. We compare and contrast: (i) standard Taylor-expanded amplitudes (top panel), (ii) new-resummed amplitudes when factoring $\mathcal{J}$ (middle panel), and (iii) new-resummed amplitude when factoring $H_{\rm eff}$ (bottom panel). For brevity, the "standard Taylor-expanded" top panel exhibits only the integer-order PN approximants. Note again, as in the case of $|\hat{h}_{22}|$ discussed above, how the use of a standard 1PN-accurate Taylor-expanded waveform leads to a grossly inaccurate approximation to the exact result, building up to -22% at the LSO. By contrast, our new-resummed $T_1[\rho_{21}^J]$-based approximant (middle panel) or, for that matter, the $T_1[\rho_{21}^H]$-based one (bottom panel), captures both qualita-

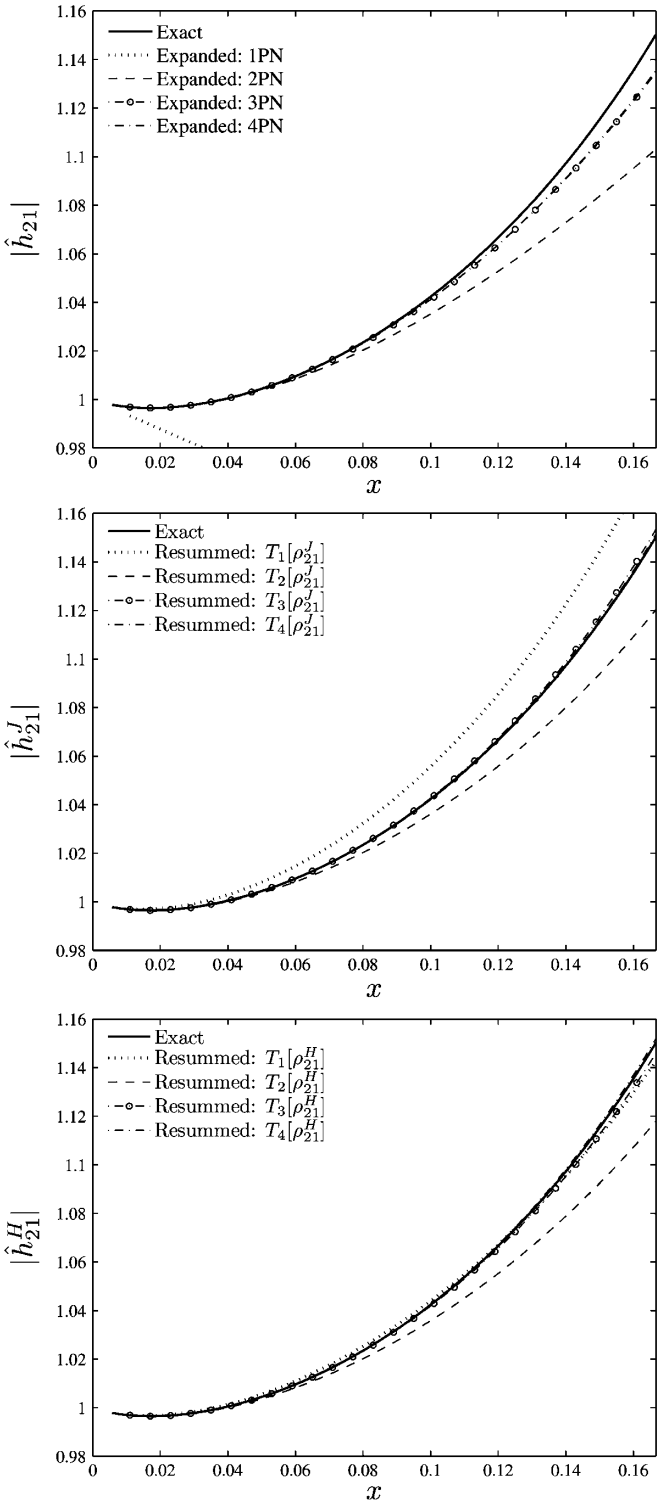

FIG. 8. Extreme-mass-ratio limit ($\nu = 0$): various representations of the $|\hat{h}_{21}|$ waveform modulus. Top panel: standard PN expansion. Middle panel: resummation factoring the angular momentum $\mathcal{J}$. Bottom panel: resummation factoring the energy $H_{\rm eff}$.

[19] As before, the fact that the resummed $T_3[\rho_{22}]$ approximant is closer to the exact result than the $T_4[\rho_{22}]$ and $T_5[\rho_{22}]$ ones is probably coincidental. It is more important to note that panel (d) exhibits much less scatter than panel (c).

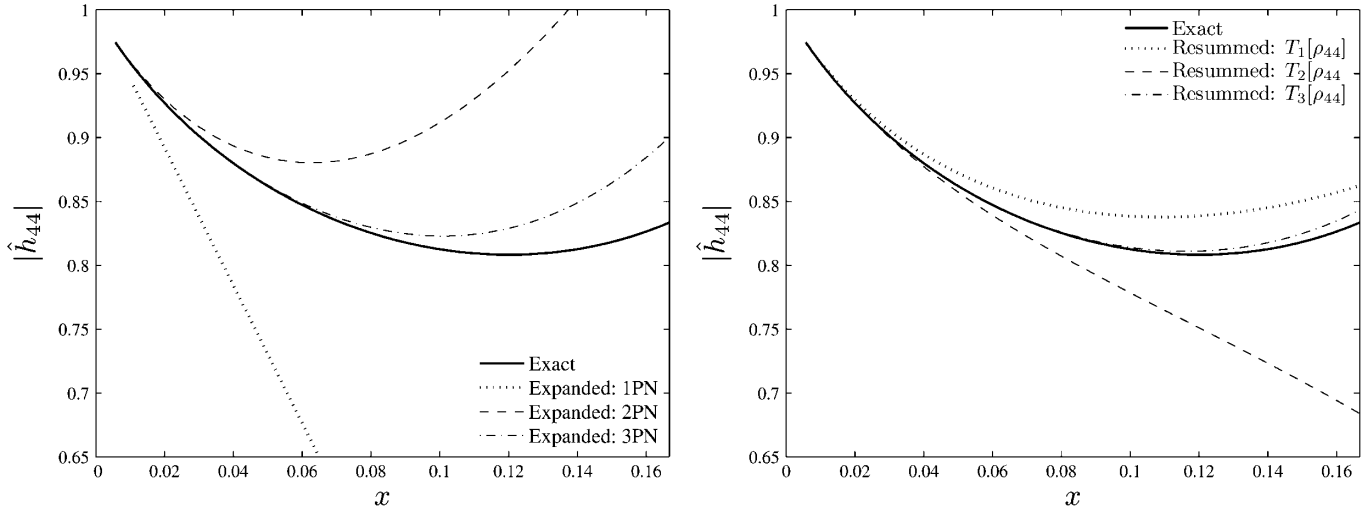

FIG. 9. Extreme-mass-ratio limit ($\nu = 0$): various representation of the $|\hat{h}_{44}|$ waveform modulus. Left panel: standard PN expansion. Right panel: our new resummation.

tively and quantitatively the correct behavior of the exact waveform.[20] Ultimately, for 3PN and 4PN accuracies, both resummed waveforms exhibit a very close agreement (within $\sim 3 \times 10^{-3}$ for the $\mathcal{J}$ case) with the exact one. The standard Taylor-expanded ones are also close to the exact results, but visibly less close than our new approximants.

Finally, Fig. 9 exhibits the results for the $|\hat{h}_{44}|$ waveforms. Note that $\hat{h}_{44}$ and $\hat{h}_{42}$ are the last partial multipoles for which the analytical $\nu = 0$ result is known to 3PN accuracy. The comparisons between standard Taylor-expanded and new-resummed waveforms displayed in Fig. 9 leads to essentially the same conclusions as above. In particular, the standard Taylor-expanded 1PN accurate waveform is even more grossly inaccurate[21] than before, as the difference builds up to about -90% at the LSO (i.e., $|\hat{h}^{\rm 1PN}_{44}(x_{\rm LSO})| \approx 0.0793$ instead of $|\hat{h}^{\rm Exact}_{44}|(x_{\rm LSO}) = 0.8334$)! Let us also emphasize that, as we could have already pointed out for $|\hat{h}_{22}|$ and for $|\hat{h}_{21}|$, the new-resummed approximant based on the 2PN-accurate Taylor-expanded $\rho_{\ell m}$'s is systematically less good than the one based on the 1PN-accurate Taylor-expanded $\rho_{\ell m}$'s. This suggests that for waveforms that are subdominant with respect to h_{44} and h_{42} (for which one does not know the 3PN expansion of the waveform) one will be better off, if one intends to use Taylor-expanded $\rho_{\ell m}$'s, in employing only the 1PN accurate $\rho_{\ell m}$'s. However, as we have shown in the $\ell = m = 2$ case (see Table II and Fig. 7), we expect that a suitable Padé resummation of the highest accuracy available results will yield better agreement than simply using the Taylor 1PN-accurate $\rho_{\ell m}$'s. In this respect, let us recall that, as exhibited in Eqs. (45) and (46), the 1PN corrections for all even- and odd-parity multipoles are known. In the $\nu \to 0$ limit they are given by Eqs. (45) and (46); in the comparable-mass case the even-parity result is given by Eq. (41), while the odd-parity result is given in Appendix A.

IV. RESULTS FOR THE COMPARABLE-MASS CASE (NOTABLY THE EQUAL-MASS CASE, $\nu = 0.25$)

Let us continue to test our resummation procedure by considering the comparable-mass case $\nu \neq 0$, and notably the equal-mass case, $\nu = 1/4 = 0.25$. In this case, we cannot rely on the knowledge of the exact multipolar waveforms from comparable-mass circular orbits. Indeed, though this problem can in principle be numerically investigated for binary black-hole systems by considering the helical Killing-vector approach (see Ref. [34] and references therein), there are no presently available results where one goes beyond the conformally flat approximation to Einstein equations. (But see Ref. [35] for the case of binary neutron star systems.) For what concerns the available numerical results on coalescing black holes, previous work has shown that the deviations from the adiabatic-quasi-circular approximation were far from being negligible near the LSO, so that they cannot be directly compared to the circular waveforms investigated in this paper. We leave to future work a comparison between suitably non-quasi-circular corrected analytical waveforms and the results of numerical simulations of coalescing black holes.

In the absence of exact waveforms to be compared to, we shall content ourselves here by investigating the inner *consistency* and *robustness* of our current best-bet analyti-

[20]The fact that the resummed $T_1[\rho^H_{21}]$-based approximant is extremely close to the exact result (see bottom panel) is probably coincidental. We do not expect this coincidence to hold for higher-order partial waves.

[21]This is the consequence of the analytical fact noted above that the 1PN correction to the waveform is negative and grows linearly with ℓ. We recall that this fact was one of our motivations for introducing the new quantities $\rho_{\ell m}$.

cal approximants as suggested by the $\nu = 0$ results reported above. More precisely, we shall study the dependence of $\rho_{\ell m}$ and the corresponding new-resummed waveform $|\hat{h}_{\ell m}|$ on the two EOB deformation parameters ν and a_5.

A. Mild dependence of $\rho_{\ell m}$ on ν

To motivate the study of the ν dependence of $\rho_{\ell m}$ let us start by having a close look at the general structure of $\rho_{\ell m}$, i.e.,

$$\rho_{\ell m}(x;\nu) = 1 + c_1^{\rho_{\ell m}}(\nu)x + c_2^{\rho_{\ell m}}(\nu)x + c_3^{\rho_{\ell m}}(\log(x);\nu)x^3 + \ldots. \tag{61}$$

For concreteness, let us display here $\rho_{44}(x;\nu)$ (given together with our results in Appendix C)

$$\rho_{44}(x;\nu) = 1 + \frac{2625\nu^2 - 5870\nu + 1614}{1320(3\nu - 1)}x + \frac{1\,252\,563\,795\nu^4 - 6\,733\,146\,000\nu^3 - 313\,857\,376\nu^2 + 2\,338\,945\,704\nu - 511\,573\,572}{317\,116\,800(1 - 3\nu)^2}x^2 + \left(\frac{16\,600\,939\,332\,793}{1\,098\,809\,712\,000} - \frac{12\,568}{3\,465}\text{eulerlog}_4(x)\right)x^3. \tag{62}$$

We see on the example of ρ_{44} that the ν dependence of the coefficient $c_n^{\rho_{\ell m}}(\nu)$ is not polynomial in ν, but rather given by a rational fraction. The denominator of this rational fraction in the case of ρ_{44} is proportional to some power of $1 - 3\nu$. The denominator $1 - 3\nu$ decreases significantly (from 1 to 1/4) as ν increases from the extreme-mass-ratio case, $\nu = 0$, to the equal-mass case, $\nu = 1/4$. From Eq. (7), for the general multipole $\rho_{\ell m}^{(\epsilon)}$ this denominator would be proportional to a power of

$$d_{\ell m}(\nu) = \frac{c_{\ell+\epsilon}(\nu)}{X_2 + (-)^m X_1} = \frac{X_2^{\ell+\epsilon-1} + (-)^m X_1^{\ell+\epsilon-1}}{X_2 + (-)^m X_1}. \tag{63}$$

This ratio is expressible as a polynomial in ν. For instance, for ρ_{54}, it would be $d_{54} = 1 - 5\nu + 5\nu^2$, which decreases from 1 down to 1/16 as ν goes from 0 to 1/4. More generally, $d_{\ell m}(\nu)$ decreases, as ν varies from 0 to 1/4, from 1 down to $1/2^{\ell+\epsilon-2}$ when $\pi(m) = 0$ and to $(\ell + \epsilon - 1)/2^{\ell+\epsilon-2}$, when $\pi(m) = 1$. The presence of such "small denominators" raises the issue of a possible large increase of the coefficients $c_n^{\rho_{\ell m}}(\nu)$ as ν increases from 0 to 1/4. If that were true, this would undermine the applicability to the comparable-mass case of the conclusions that we have drawn above from the $\nu \to 0$ limit. Therefore, we have studied the ν dependence of the known coefficients $c_n^{\rho_{\ell m}}(\nu)$ to check whether the presence of these "small denominators" might cause them to grow uncontrollably when ν increases. In Table IV we list the fractional differences $\bar{\Delta}c_n^{\rho_{\ell m}}(\nu) = c_n^{\rho_{\ell m}}(\nu)/c_n^{\rho_{\ell m}}(0) - 1$ at $\nu = 1/4$ (and at $\log(x) = \log(1/6)$ for the logarithms contained in the higher coefficients) for a sample of the $\rho_{\ell m}$'s whose ν dependence is analytically known. The good news is that Table IV indicates that the fractional variation of the coefficients $c_n^{\rho_{22}}(\nu)$ when going from the extreme-mass ratio case to the equal-mass ratio one is typically of the order of 20%.

TABLE IV. Analysis of the fractional variation $\bar{\Delta}c_n^{\rho_{\ell m}}(\nu) = c_n^{\rho_{\ell m}}(\nu)/c_n^{\rho_{\ell m}}(0) - 1$ of the coefficients $c_n^{\rho_{\ell m}}(\nu)$ in Eq. (61) for a selected sample of values of (ℓ, m).

(ℓ, m)	$\bar{\Delta}c_1^{\rho_{\ell m}}(1/4)$	$\bar{\Delta}c_2^{\rho_{\ell m}}(1/4)$	$\bar{\Delta}c_3^{\rho_{\ell m}}(1/4, \log(1/6))$
(2, 2)	−0.159 884	0.185 947	−0.100 421
(4, 4)	−0.230 328	0.46 265	...
(5, 4)	−0.176 295	...	...

This mild dependence of the coefficients $c_n^{\rho_{\ell m}}(\nu)$ on ν is the basis of the proposal [2] of improving the accuracy of known ν-dependent $\rho_{\ell m}$'s by adding the $\nu \to 0$ limit of higher-order PN corrections (hybridization). [For instance, in the case of $\rho_{22}(x;\nu)$, where the ν-dependent terms are known up to 3PN, we have added the 4PN and 5PN $\nu = 0$ corrections.] Indeed, this procedure consists in using, for some higher corrections, the *approximation*[22] $c_n^{\rho_{\ell m}}(\nu) \approx c_n^{\rho_{\ell m}}(0)$.

We have validated this approximate completion of known ν-dependent terms in the following way. In view of the results of Table IV, we have tested our procedure by modifying the 4PN coefficient for $\nu = 0$, $c_4^{\rho_{22}}(0)$, by multiplying it by the factor $(1 + 0.8\nu)$, in order to mimic a possible 20% increase of this coefficient when ν increases up to 1/4. We then found that such a modification of the 4PN coefficient yielded a corresponding modification of $T_5[\rho_{22}(x;\nu)]$ equal to $T_5[\rho_{22}(x;\nu)]^{\text{modified}}/T_5[\rho_{22}(x;\nu)] = 1.00\,038$ when evaluated for $\nu = 0.25$ at $x = 1/6$. Even at $x = 1/3$ we find that such a modification yields

[22]Note that our results on the mild ν dependence of $c_n^{\rho_{\ell m}}(\nu)$ show that, *a contrario*, a naive hybridization of the waveform of the type $\hat{h}_{\ell m}^{\text{hybrid}} = \hat{h}_{\ell m}^{\text{known}}(\nu) + \hat{h}_{\ell m}^{\text{higher}}(\nu = 0)$ would probably be rather unreliable, especially for $\ell \geq 3$, because it would not incorporate the overall strong decrease approximately proportional to the "small denominator" $d_{\ell m}(\nu)$, Eq. (63).

$T_5[\rho_{22}(x;\nu)]^{\rm modified}/T_5[\rho_{22}(x;\nu)] = 1.013$. In the ρ_{44} case, where the ν-dependent corrections are known only up to 2PN accuracy, a similar modification of the 3PN term for $\nu = 0$ by a factor $(1 + 0.8\nu)$ yields a corresponding fractional change of ρ_{44} between $\nu = 0$ and $\nu = 0.25$ equal to 1.0099 at $x = 1/6$ and 1.079 at $x = 1/3$. These results confirm the reliability of the hybridization procedure adopted here, and give us an idea of the related small uncertainty. For instance, for the dominant quadrupolar wave, we can anticipate that our hybridization procedure introduces an uncertainty in the waveform $h_{22}(x) \propto (\rho_{22}(x))^2$ of order 8×10^{-4} at the LSO. This level of uncertainty is comparable to the fractional difference between our best-bet quadrupolar amplitude based on $P^2_3[\rho_{22}(x, \nu = 0)]$ and the exact result (see Table II).

B. Mild sensitivity of $|\hat{h}_{\ell m}|$ to ν

In Fig. 5 we had put together, in the extreme-mass-ratio case, the predictions for $|\hat{h}_{22}|$ made by all the higher-order approximants within our new resummation method. Let us now deform the results of Fig. 5 by turning on ν and increasing it up to $\nu = 1/4$. Figure 10 is the "$\nu = 1/4$-deformed" version of Fig. 5. In constructing this figure we have used the value $a_5 = 0$ for the 4PN EOB parameter entering Eq. (11), and we have defined the EOB radial potential $A(u)$ as being $P^1_4[A^{\rm Taylor}(u; a_5)]$. The horizontal axis has been extended up to the location of $x_{\rm LSO}(a_5, \nu)$ as predicted by the corresponding adiabatic EOB dynamics, namely, $x_{\rm LSO}(0, 1/4) = 0.2112$. Some of the lessons we might draw from comparing the $\nu = 1/4$-deformed Fig. 10 to its $\nu = 0$ counterpart, Fig. 5, are the following: (i) apart from $P^4_1\{T_5[\rho_{22}]\}$ (which still has a spurious pole) and our old $P^3_2\{f_{22}\}$, the *relative stacking order* of *all* the other approximants is maintained in the deformation between $\nu = 0$ and $\nu = 1/4$; (ii) our old prescription [1,2] based on $P^3_2\{f_{22}\}$, which in the $\nu = 0$ case was clustered together with the other approximants (as well as with the exact curve), seems now to have drifted apart from the cluster of the other ones; (iii) indeed, all the new approximants are rather well clustered together, with a dispersion which reaches only about 2% at $x_{\rm LSO}(0, 1/4) = 0.2112$.

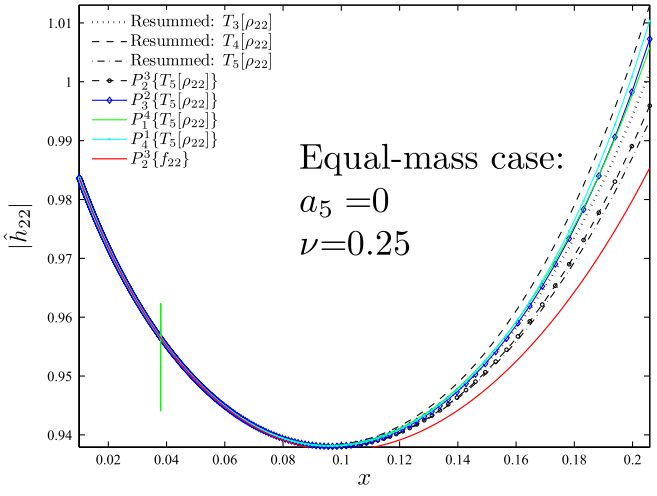

FIG. 10 (color online). Equal-mass case ($\nu = 1/4$): contrasting various methods for resumming the waveform modulus $|\hat{h}_{22}|$ for $a_5 = 0$. Note the presence of a localized spurious pole in $P^4_1\{T_5[\rho_{22}]\}$ at $x \approx 0.038$.

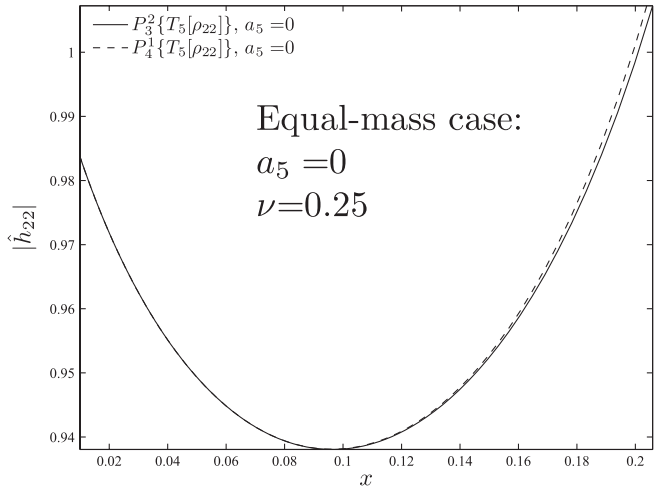

FIG. 11. Equal-mass case ($\nu = 1/4$): Same as Fig. 10, but focussing on only the "best" (3^{+2}PN-accurate) Padé approximants to the waveform.

One of the results of the $\nu = 0$ study above, particularly in the dominant $\ell = m = 2$ case, was to select, among the array of new approximants, a small sample of "best approximants." This sample was made of the approximants based on $P^2_3\{T_5[\rho_{22}]\}$ and $P^1_4\{T_5[\rho_{22}]\}$. In Fig. 11 we extracted from the previous figure the $\nu = 1/4$-deformed version of only these two "best approximants." Remembering that in the $\nu = 0$ case these two curves were both extremely close (within 6×10^{-9} at $x = 1/6$!) to each other, as well as being very close to the correct answer, we note that their $\nu = 1/4$-deformed versions are still very close to each other (within 3×10^{-3} at $x_{\rm LSO}(0, 1/4) = 0.2112$). We therefore expect that this doublet of curves is a good indication of where the currently unknown (circular, adiabatic) correct $\nu = 1/4$ curve might lie.

C. Weak dependence of $|\hat{h}_{\ell m}(x)|$ on a_5

Finally, we study in Fig. 12 the sensitivity of our new-resummed *circular waveform* to the 4PN EOB parameter a_5. This sensitivity comes from several sources. Both the source term $S^{(\epsilon)}_{\rm eff}$ in Eq. (1) and the tail term $T_{\ell m}$ depend on the EOB dynamical quantities H and $\mathcal{J}$. Therefore, when expressing the waveform as a function of the frequency parameter x, obtained by solving Eq. (13) above, the a_5-dependent radial potential $A(u)$ comes in at several different places.

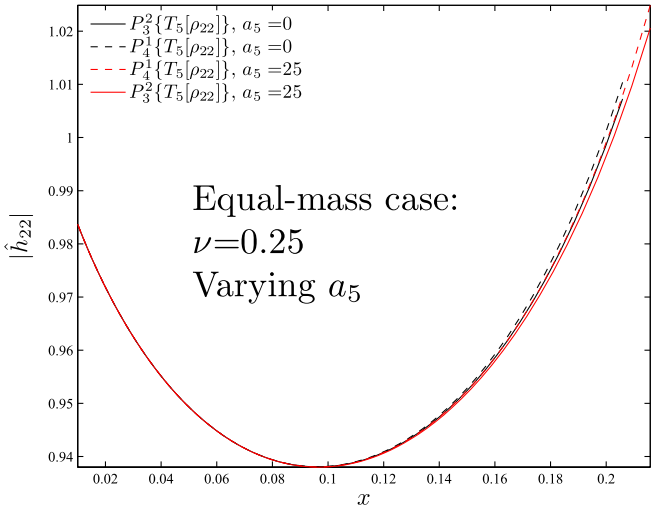

FIG. 12 (color online). Equal-mass case ($\nu = 1/4$): Effect of varying a_5 (between 0 and 25) on the best Padé approximants displayed in Fig. 11.

For concreteness, we shall study the "deformation" of our two best approximants when a_5 increases from 0 to 25 (such a range is motivated by recent work [2,10,11,18]). The a_5-deformed version of Fig. 11 is plotted as Fig. 12. This figure compares two doublets of curves: our two best Padé approximants ($P_3^2\{T_5[\rho_{22}]\}$, $P_4^1\{T_5[\rho_{22}]\}$) for $a_5 = 0$ versus the same Padé approximants when $a_5 = 25$.

The main thing to note is that the a_5 deformation is continuous and monotonic. The displacement of each curve is only of order 2×10^{-3} at $x = 0.2112 = x_{\rm LSO}(0, 1/4)$ (the horizontal axis of the figure has been extended up to $x_{\rm LSO}(25, 1/4) = 0.2236$). In addition, the separation of the a_5-deformed doublet of Padé curves is about the same as it was before deformation.

V. CONCLUSIONS

In this paper we have explored the properties of a new resummation method of post-Newtonian multipolar waveforms from circular nonspinning compact binaries. The two characteristic features of this method are (i) the *multiplicative* decomposition of the (complex) $h_{\ell m}^{(\epsilon)}$ waveform into the product of several factors corresponding to various physical effects, and (ii) the replacement of the last (real) factor, $f_{\ell m}$, in this decomposition, by its ℓ-*th root* $\rho_{\ell m}(x) = (f_{\ell m}(x))^{1/\ell}$.

To test this resummation method we have first considered the extreme-mass-ratio limit ($\nu \to 0$), for which exact results for the waveform can be obtained by numerical analysis of black-hole perturbation theory. We first noted (see Fig. 3) that the new quantity that we introduced, $\rho_{\ell m}(x)$, has a remarkably simple quasilinear behavior as a function of the orbital frequency parameter $x = (GM\Omega/c^3)^{2/3}$. [In the odd-parity case, this quasilinear behavior is especially pronounced when factoring out the angular momentum $\mathcal{J}$ from the wave amplitude. This leads us to consider $\rho_{\ell m}^J$ as our "best-bet" default choice.] We related the simple properties of the function $\rho_{\ell m}(x)$ [including those concerning its dependence on (ℓ, m)], to analytical results on the 1PN corrections to multipole moments. In this regard, we explicitly computed new expressions for the 1PN source current multipoles for arbitrary ℓ and in consequence the coefficient of the 1PN correction in the *odd-parity* waveform (and $\rho_{\ell m}$). The quasilinear behavior of the functions $\rho_{\ell m}(x)$ also means that 2PN and higher-order corrections to them are smaller than analogous corrections in usual quantities, like the waveform.

We have shown that, even if one uses only (without any further resummation) the successive Taylor approximants to $\rho_{\ell m}$, this defines a sequence of *new-resummed approximants* to the waveform which "converges" toward the exact waveform much less erratically than the standard PN-approximants. Moreover, for all the waveforms for which 3PN corrections are known (at least when $\nu \to 0$), our results show that the new-resummed waveform nearly coincide with the exact results starting with the 3PN approximation (see Figs. 6, 8, and 9). We have also shown that we can further improve the quality of our new approximants by suitably Padé-resumming the function $\rho_{\ell m}(x)$ before using it to construct the waveform $h_{\ell m}^{(\epsilon)}(x) \propto (\rho_{\ell m}(x))^\ell$. In particular, two Padé approximants to ρ_{22}, namely, $P_3^2\{T_5[\rho_{22}]\}$ and $P_4^1\{T_5[\rho_{22}]\}$, stand out as defining the most accurate representation of the exact waveform (see Fig. 7).

We have finally explored the robustness of our approximants when considering a finite mass ratio. We have checked that the ν dependence of the coefficients entering the Taylor expansion of the function $\rho_{\ell m}(x; \nu)$ is rather mild in spite of the presence of ν-dependent denominators that decrease very significantly as ν increases from 0 to $1/4$. This justifies the proposal of completing the known ν-dependent $\rho_{\ell m}$'s by adding the $\nu \to 0$ limit of higher-order PN corrections. We have also shown that the relative stacking order of all the best approximants is maintained in the "ν deformation" between $\nu = 0$ and $\nu = 1/4$. In addition, our new approximants are rather well clustered together, with a dispersion which reaches only about 2% at the last stable orbit.

Let us finally note that we have compared in the four panels of Fig. 1 four different resummation approaches to the total (Newton-normalized) GW energy flux $\hat{F}(x)$ (for $\nu \to 0$): (a) the standard post-Newtonian (Taylor) expansion, (b) the Padé resummation advocated long ago [6], (c) the improved $v_{\rm pole}$-tuned Padé resummation advocated in [2], and (d) our present new resummation method (using only Taylor-expanded $\rho_{\ell m}$'s). The $v_{\rm pole}$-flexed technique, panel (c), is clearly superior to the results of the first two techniques, panels (a) and (b). It has however the disadvantage that it needs to rely on some external knowledge (such as the exact value of the flux at the LSO) to determine

the optimal value of $v_{\rm pole}$. On the other hand, our new resummation procedure not only stands out, among all other proposals, as yielding the best agreement with the exact flux (when $\nu = 0$), but it has also the further advantage of being parameter-free.

ACKNOWLEDGMENTS

We are grateful to E. Berti for kindly providing us with his frequency-domain numerical data. The activity of A. Nagar at Institut des Hautes Etudes Scientifiques (IHES) is supported by INFN. B. R. Iyer thanks IHES and the Institut d'Astrophysique de Paris for hospitality and support during different stages of this work.

APPENDIX A: RESULTS FOR ODD-PARITY (CURRENT) 1PN-ACCURATE MULTIPOLES

The 1PN-accurate results for the source current (i.e., odd-parity) moments (of any multipolar order ℓ) were obtained long ago in Eqs. (5.18) and/or (5.21) of Ref. [31]. Alternatively, we can use as starting point for the explicit determination of the 1PN-accurate source current-multipole moment Eqs. (4.3) and (4.4) in [36]. Recalling the notation $\gamma = GM/Rc^2$ and (consistently with Eq. (7)) using the notation

$$b_\ell(\nu) \equiv X_2^\ell + (-)^\ell X_1^\ell, \tag{A1}$$

$$c_\ell(\nu) \equiv X_2^{\ell-1} + (-)^\ell X_1^{\ell-1}, \tag{A2}$$

$${}_cY_b^L(\mathbf{y}_1, \mathbf{y}_2) \equiv \frac{\partial}{\partial y_1^c}\frac{\partial}{\partial y_2^b} Y^L(\mathbf{y}_1, \mathbf{y}_2), \tag{A3}$$

$$Y^L(\mathbf{y}_1, \mathbf{y}_2) \equiv \frac{r_{12}}{\ell+1}\sum_{p=0}^{\ell} y_1^{\langle L-P} y_2^{P\rangle}, \tag{A4}$$

at 1PN accuracy the "compact" terms for the source current-multipole moment J_L can be explicitly evaluated, in the circular orbit case, for a general value of ℓ (as in the $\ell + m$ even case). They read

$$J_L^{\rm compact} = STF_L \nu M \epsilon_{abi_\ell} x_a v_b \Big\{ x^{L-1}\Big[c_{\ell+1}(\nu) + \gamma(b_{\ell+1}(\nu) + 2\nu b_{\ell-1}(\nu) + \Big(\frac{1}{2} - \frac{(\ell-1)(\ell+4)}{2(\ell+2)(2\ell+3)}\Big)c_{\ell+3}(\nu))\Big] + \frac{r^2}{c^2} x_{L-3} v_{i_{\ell-2}} v_{i_{\ell-1}} \frac{(\ell-1)(\ell-2)(\ell+4)}{2(\ell+2)(2\ell+3)} c_{\ell+3}(\nu)\Big\}. \tag{A5}$$

In addition to the above "compact terms"(generated by compact-support terms in the effective stress-energy tensor $\tau^{\mu\nu}$), there exist three "noncompact" contributions that make the 1PN current moments more involved than the corresponding 1PN mass moments. These noncompact contributions can be expressed in terms of the Y^L objects introduced in [31], so as to obtain,

$$J_L^{\rm noncompact} = STF_L \nu M \epsilon_{abi_\ell} \frac{GM}{c^2} \times \Big[2X_1 v^c {}_cY_b^{L-1a} + \frac{3}{2} X_2 v^c {}_cY_b^{L-1a} - \frac{2\ell+1}{2(\ell+2)(2\ell+3)} \frac{d}{dt}({}_aY_c^{L-1cb}) + 1 \leftrightarrow 2\Big]. \tag{A6}$$

More explicit expressions for these noncompact contributions can be provided for a general value of ℓ by straightforward but slightly long computations. For circular orbits one can check that the last term does not contribute and the final result for the other two terms can be simply re-expressed in terms of the polynomials $b_\ell(\nu)$ and $c_\ell(\nu)$, Eqs. (A1) and (A2), as for the compact terms. The final result (for circular orbits) is given by

$$J_L^{\rm noncomp} = STF_L \nu M \gamma \epsilon_{abi_\ell} x_a v_b x^{L-1} \times \Big[\frac{c_{\ell+3}(\nu) + 3b_{\ell+1}(\nu)}{2\ell} + \nu \frac{4b_{\ell-1}(\nu) - c_{\ell+1}(\nu)}{2\ell}\Big]. \tag{A7}$$

In the test-mass limit ($\nu \to 0$) this expression reduces to

$$J_L^{\rm noncomp} = STF_L 2\nu M \gamma \epsilon_{abi_\ell} x_a v_b x^{L-1} \frac{(-1)^{l+1}}{\ell}. \tag{A8}$$

Thus, in the circular orbit case, the 1PN-accurate current-multipole for a general value of ℓ finally reads

$$J_L = STF_L \nu M \epsilon_{abi_\ell} x_a v_b \Big\{ x^{L-1}\Big[c_{\ell+1}(\nu) + \gamma\Big(-\frac{\nu}{2\ell} c_{\ell+1}(\nu) + \frac{2\ell+3}{2\ell} b_{\ell+1}(\nu) + 2\nu \frac{\ell+1}{\ell} b_{\ell-1}(\nu) + \frac{1}{2}\Big(\frac{\ell+1}{\ell} - \frac{(\ell-1)(\ell+4)}{(\ell+2)(2\ell+3)}\Big)c_{\ell+3}(\nu)\Big)\Big] + \frac{r^2}{c^2} x_{L-3} v_{i_{\ell-2}} v_{i_{\ell-1}} \frac{(\ell-1)(\ell-2)(\ell+4)}{2(\ell+2)(2\ell+3)} c_{\ell+3}(\nu)\Big\}. \tag{A9}$$

Adapting the reasoning line of Ref. [12], recalling the additional velocity dependence of the current moments that leads to $(v/c)^{\ell+1}$ and noting that $\gamma = x$ to this order of accuracy, one can finally show that, for circular orbits, the 1PN-accurate odd-parity $\hat{h}^{(1)}_{\ell m}$'s read

$$\hat{h}^{(1)}_{\ell m}(x;\nu) = 1 - x\Big\{(\ell+1)\Big(1-\frac{\nu}{3}\Big) + \frac{\nu}{2\ell} - \frac{2\ell+3}{2\ell}\frac{b_{\ell+1}(\nu)}{c_{\ell+1}(\nu)} - 2\nu\frac{\ell+1}{\ell}\frac{b_{\ell-1}(\nu)}{c_{\ell+1}(\nu)} - \frac{1}{2}\frac{\ell+1}{\ell}\frac{c_{\ell+3}(\nu)}{c_{\ell+1}(\nu)} + \frac{m^2(\ell+4)}{2(\ell+2)(2\ell+3)}\frac{c_{\ell+3}(\nu)}{c_{\ell+1}(\nu)}\Big\} + \mathcal{O}(x^2), \tag{A10}$$

where we have not simplified on purpose in order to allow the reader to explicitly track the origin of each single contribution. In the extreme-mass-ratio limit, $M \equiv m_1 \gg \mu \equiv m_2$ $(\nu \equiv \mu/M \to 0)$, one has $c_\ell(0) = b_\ell(0) = (-1)^\ell$, and so this equation simply reduces to

$$\hat{h}^{(1)}_{\ell m}(x;0) = 1 - x\Big(\ell - \frac{1}{2} - \frac{2}{\ell} + \frac{m^2(\ell+4)}{2(\ell+2)(2\ell+3)}\Big) + \mathcal{O}(x^2). \tag{A11}$$

When computing the amplitude $f^J_{\ell m}(x;\nu)$ (where $\hat{S}^{(1,J)}_{\rm eff} \equiv \hat{j}$ is factorized), an additional contribution of $-(3/2 + \nu/6)x$ [see Eq. (18)] comes in, so that the 1PN-accurate $f^J_{\ell m}(x;\nu)$'s read

$$f^J_{\ell m}(x;\nu) = 1 - x\Big\{(\ell+1)\Big(1-\frac{\nu}{3}\Big) + \frac{3}{2} + \frac{\nu}{6} + \frac{\nu}{2\ell} - \frac{2\ell+3}{2\ell}\frac{b_{\ell+1}(\nu)}{c_{\ell+1}(\nu)} - 2\nu\frac{\ell+1}{\ell}\frac{b_{\ell-1}(\nu)}{c_{\ell+1}(\nu)} - \frac{1}{2}\frac{\ell+1}{\ell}\frac{c_{\ell+3}(\nu)}{c_{\ell+1}(\nu)} + \frac{m^2(\ell+4)}{2(\ell+2)(2\ell+3)}\frac{c_{\ell+3}(\nu)}{c_{\ell+1}(\nu)}\Big\} + \mathcal{O}(x^2). \tag{A12}$$

In the test-mass limit, this equation becomes

$$f^J_{\ell m}(x;0) = 1 - x\Big(\ell + 1 - \frac{2}{\ell} + \frac{m^2(\ell+4)}{2(\ell+2)(2\ell+3)}\Big) + \mathcal{O}(x^2). \tag{A13}$$

These results lead to the 1PN-accurate $\rho^J_{\ell m}$'s, Eqs. (46) and (49), that we have used in this paper.

For completeness, we conclude this appendix by quoting the ν-dependent, 1PN-accurate $f_{\ell m}$'s for $\ell + m$ even and a ready-reckoner of the $b_\ell(\nu)$ and $c_\ell(\nu)$ functions for ℓ values relevant for this work, Table V. From Eq. (C5) of Ref. [12], the general expression of $\hat{h}^{(0)}_{\ell m}$ at 1PN reads

$$\hat{h}^{(0)}_{\ell m}(x;\nu) = 1 - x\Big\{\ell\Big(1-\frac{\nu}{3}\Big) - \frac{3}{2}\frac{c_{\ell+2}(\nu)}{c_\ell(\nu)} + \frac{b_\ell(\nu)}{c_\ell(\nu)} + \frac{c_{\ell+2}(\nu)}{c_\ell(\nu)}\frac{m^2(\ell+9)}{2(\ell+1)(2\ell+3)}\Big\} + \mathcal{O}(x^2). \tag{A14}$$

From this expression, the even-parity $f_{\ell m}$'s follow as

$$f_{\ell m}(x;\nu) = 1 - x\Big\{\ell\Big(1-\frac{\nu}{3}\Big) - \frac{1}{2} - \frac{3}{2}\frac{c_{\ell+2}(\nu)}{c_\ell(\nu)} + \frac{b_\ell(\nu)}{c_\ell(\nu)} + \frac{c_{\ell+2}(\nu)}{c_\ell(\nu)}\frac{m^2(\ell+9)}{2(\ell+1)(2\ell+3)}\Big\} + \mathcal{O}(x^2), \tag{A15}$$

which reduces to Eq. (43) in the test-mass limit.

APPENDIX B: EXPLICIT FORM OF THE $f_{\ell m}$'S WITH HIGHER PN-ACCURACY

In this appendix we complete the information given in the text by explicitly listing the $f_{\ell m}$'s that are known at an accuracy higher than 1PN. This means considering multi-

TABLE V. List of the $b_\ell(\nu)$ and $c_\ell(\nu)$ functions that appear in the text for some values of ℓ. In the following formulas, we have introduced the notation $X_{12} \equiv X_1 - X_2 = \mathrm{sign}(m_1 - m_2)\sqrt{1-4\nu}$.

ℓ	$b_\ell(\nu)$	$c_\ell(\nu)$
1	$-X_{12}$	0
2	$1-2\nu$	1
3	$-X_{12}(1-\nu)$	$-X_{12}$
4	$1-4\nu+2\nu^2$	$1-3\nu$
5	$-X_{12}(1-3\nu+\nu^2)$	$-X_{12}(1-2\nu)$
6	$1-6\nu+9\nu^2-2\nu^3$	$1-5\nu+5\nu^2$
7	$-X_{12}(1-5\nu+6\nu^2-\nu^3)$	$-X_{12}(1-4\nu+3\nu^2)$
8	$1-8\nu+20\nu^2-16\nu^3+2\nu^4$	$1-7\nu+14\nu^2-7\nu^3$
9	$-X_{12}(1-7\nu+15\nu^2-10\nu^3+\nu^4)$	$-X_{12}(1-6\nu+10\nu^2-4\nu^3)$
10	$1-10\nu+35\nu^2-50\nu^3+25\nu^4-2\nu^5$	$1-9\nu+27\nu^2-30\nu^3+9\nu^4$
11	$-X_{12}(1-9\nu+28\nu^2-35\nu^3+15\nu^4-\nu^5)$	$-X_{12}(1-8\nu+21\nu^2-20\nu^3+5\nu^4)$

poles up to $\ell = 5$ for even-parity modes ($\ell + m$ even) and $\ell = 4$ for odd-parity modes ($\ell + m$ odd). We consider separately the even-parity $f_{\ell m}$'s and the odd-parity $f^J_{\ell m}$'s and $f^H_{\ell m}$'s.

1. Even-parity $f_{\ell m}$'s

The even-parity $f_{\ell m}$'s (with $\nu \neq 0$ and $\nu = 0$ contributions) are given by

$$f_{22}(x;\nu) = 1 + \frac{1}{42}(55\nu - 86)x + \frac{2047\nu^2 - 6745\nu - 4288}{1512}x^2 + \left(\frac{114\,635\nu^3}{99\,792} - \frac{227\,875\nu^2}{33\,264} + \frac{41}{96}\pi^2\nu - \frac{34\,625\nu}{3696} - \frac{856}{105}\mathrm{eulerlog}_2(x) + \frac{21\,428\,357}{727\,650}\right)x^3 + \left(\frac{36\,808}{2205}\mathrm{eulerlog}_2(x) - \frac{5\,391\,582\,359}{198\,648\,450}\right)x^4 + \left(\frac{458\,816}{19\,845}\mathrm{eulerlog}_2(x) - \frac{93\,684\,531\,406}{893\,918\,025}\right)x^5 + \mathcal{O}(x^6), \quad \text{(B1)}$$

$$f_{33}(x;\nu) = 1 + \left(2\nu - \frac{7}{2}\right)x + \left(\frac{887\nu^2}{330} - \frac{3401\nu}{330} - \frac{443}{440}\right)x^2 + \left(\frac{147\,471\,561}{2\,802\,800} - \frac{78}{7}\mathrm{eulerlog}_3(x)\right)x^3 + \left(39\mathrm{eulerlog}_3(x) - \frac{53\,641\,811}{457\,600}\right)x^4 + \mathcal{O}(x^5), \quad \text{(B2)}$$

$$f_{31}(x;\nu) = 1 + \left(-\frac{2\nu}{3} - \frac{13}{6}\right)x + \left(-\frac{247\nu^2}{198} - \frac{371\nu}{198} + \frac{1273}{792}\right)x^2 + \left(\frac{400\,427\,563}{75\,675\,600} - \frac{26}{21}\mathrm{eulerlog}_1(x)\right)x^3 + \left(\frac{169}{63}\mathrm{eulerlog}_1(x) - \frac{12\,064\,573\,043}{1\,816\,214\,400}\right)x^4 + \mathcal{O}(x^5), \phi \quad \text{(B3)}$$

$$f_{44}(x;\nu) = 1 + \frac{2625\nu^2 - 5870\nu + 1614}{330(3\nu - 1)}x + \frac{23\,740\,185\nu^3 - 106\,831\,480\nu^2 + 50\,799\,672\nu - 4\,536\,144}{1\,801\,800(3\nu - 1)}x^2 - 2\left(\frac{1\,132\,251\,120}{156\,080\,925}\mathrm{eulerlog}_4(x) - \frac{5\,992\,751\,383}{156\,080\,925}\right)x^3 + \mathcal{O}(x^4), \quad \text{(B4)}$$

$$f_{42}(x;\nu) = 1 + \frac{285\nu^2 - 3530\nu + 1146}{330(3\nu - 1)}x - \frac{2\,707\,215\nu^3 + 28\,154\,560\nu^2 - 26\,861\,688\nu + 5\,538\,096}{1\,801\,800(3\nu - 1)}x^2 - \left(\frac{1\,132\,251\,120}{312\,161\,850}\mathrm{eulerlog}_2(x) - \frac{5\,180\,369\,659}{312\,161\,850}\right)x^3 + \mathcal{O}(x^4), \quad \text{(B5)}$$

$$f_{55}(x;\nu) = 1 + \frac{512\nu^2 - 1298\nu + 487}{78(2\nu - 1)}x + \frac{50\,569}{6552}x^2 + \mathcal{O}(x^3), \quad \text{(B6)}$$

$$f_{53}(x;\nu) = 1 + \frac{176\nu^2 - 850\nu + 375}{78(2\nu - 1)}x + \frac{69\,359}{10\,920}x^2 + \mathcal{O}(x^3), \quad \text{(B7)}$$

$$f_{51}(x;\nu) = 1 + \frac{8\nu^2 - 626\nu + 319}{78(2\nu - 1)}x + \frac{28\,859}{4680}x^2 + \mathcal{O}(x^3), \quad \text{(B8)}$$

2. Odd-parity $f^J_{\ell m}$'s

Let us focus now on the odd-parity case and list the $f^J_{\ell m}$ in which the Newton-normalized angular momentum $\hat{j}$ has been factorized as an effective source. We have

$$f^J_{21}(x;\nu) = 1 + \left(\frac{23\nu}{42} - \frac{59}{28}\right)x + \left(\frac{85\nu^2}{252} - \frac{269\nu}{126} - \frac{5}{9}\right)x^2 + \left(\frac{88\,404\,893}{11\,642\,400} - \frac{214}{105}\mathrm{eulerlog}_1(x)\right)x^3 + \left(\frac{6313}{1470}\mathrm{eulerlog}_1(x) - \frac{33\,998\,136\,553}{4\,237\,833\,600}\right)x^4 + \mathcal{O}(x^5), \quad \text{(B9)}$$

$$f^J_{32}(x;\nu) = 1 + \frac{320\nu^2 - 1115\nu + 328}{90(3\nu-1)}x + \frac{39\,544\nu^3 - 253\,768\nu^2 + 117\,215\nu - 20\,496}{11\,880(3\nu-1)}x^2 + \left(\frac{110\,842\,222}{4\,729\,725} - \frac{104}{21}\mathrm{eulerlog}_2(x)\right)x^3 + \mathcal{O}(x^4), \tag{B10}$$

$$f^J_{43}(x;\nu) = 1 + \frac{(160\nu^2 - 547\nu + 222)}{44(2\nu-1)}x + \frac{225\,543}{40\,040}x^2 + \mathcal{O}(x^3), \tag{B11}$$

$$f^J_{41}(x;\nu) = 1 + \frac{(288\nu^2 - 1385\nu + 602)}{132(2\nu-1)}x + \frac{760\,181}{120\,120}x^2 + \mathcal{O}(x^3). \tag{B12}$$

3. Odd-parity $f^H_{\ell m}$'s

We finally list the odd-parity $f^H_{\ell m}$ in which the effective energy $\hat{H}_{\rm eff}$ has been factorized as an effective source. We have

$$f^H_{21}(x;\nu) = 1 + \left(\frac{5\nu}{7} - \frac{3}{28}\right)x + \left(\frac{79\nu^2}{168} - \frac{485\nu}{126} - \frac{97}{126}\right)x^2 + \left(\frac{70\,479\,293}{11\,642\,400} - \frac{214}{105}\mathrm{eulerlog}_1(x)\right)x^3 + \left(\frac{107}{490}\mathrm{eulerlog}_1(x) + \frac{9\,301\,790\,917}{1\,412\,611\,200}\right)x^4 + \mathcal{O}(x^5), \tag{B13}$$

$$f^H_{32}(x;\nu) = 1 + \frac{365\nu^2 - 590\nu + 148}{90(3\nu-1)}x + \frac{16\,023\nu^3 - 93\,976\nu^2 + 612\nu + 6192}{3960(3\nu-1)}x^2 + \left(\frac{96\,051\,082}{4\,729\,725} - \frac{104}{21}\mathrm{eulerlog}_2(x)\right)x^3 + \mathcal{O}(x^4), \tag{B14}$$

$$f^H_{43}(x;\nu) = 1 + \frac{524\nu^2 - 1135\nu + 402}{132(2\nu-1)}x - \frac{1667}{3640}x^2 + \mathcal{O}(x^3), \tag{B15}$$

$$f^H_{41}(x;\nu) = 1 + \frac{332\nu^2 - 879\nu + 338}{132(2\nu-1)}x + \frac{145\,021}{120\,120}x^2 + \mathcal{O}(x^3). \tag{B16}$$

APPENDIX C: COMPLETE EXPRESSIONS OF THE $\rho_{\ell m}$'S FOR $2 \le \ell \le 8$

We finally list the "hybridized" expressions of all the even- and odd-parity $\rho_{\ell m}$'s obtained from the corresponding $f_{\ell m}$'s with the proviso explained above that the ℓ-th power of the hybridized $\rho_{\ell m}$ presented here would generate some specific ν-dependent higher-order coefficients $c^{f_{\ell m}}_{n'}(\nu)$, which differ from the $c^{f_{\ell m}}_{n'}(\nu=0)$ listed in, e.g., the equations of Appendix B. In the odd-parity case, we only list the $\mathcal{J}$-normalized $\rho^J_{\ell m}$'s obtained from the $f^J_{\ell m}$'s. For completeness and future reference we present the $\rho_{\ell m}$'s explicitly up to $\ell = 8$ included.

$$\rho_{22}(x;\nu) = 1 + \left(\frac{55\nu}{84} - \frac{43}{42}\right)x + \left(\frac{19\,583\nu^2}{42\,336} - \frac{33\,025\nu}{21\,168} - \frac{20\,555}{10\,584}\right)x^2 + \left(\frac{10\,620\,745\nu^3}{39\,118\,464} - \frac{6\,292\,061\nu^2}{3\,259\,872} + \frac{41\pi^2\nu}{192} - \frac{48\,993\,925\nu}{9\,779\,616} - \frac{428}{105}\mathrm{eulerlog}_2(x) + \frac{1\,556\,919\,113}{122\,245\,200}\right)x^3 + \left(\frac{9202}{2205}\mathrm{eulerlog}_2(x) - \frac{387\,216\,563\,023}{160\,190\,110\,080}\right)x^4 + \left(\frac{439\,877}{55\,566}\mathrm{eulerlog}_2(x) - \frac{16\,094\,530\,514\,677}{533\,967\,033\,600}\right)x^5 + \mathcal{O}(x^6), \tag{C1}$$

$$\rho^J_{21}(x;\nu) = 1 + \left(\frac{23\nu}{84} - \frac{59}{56}\right)x + \left(\frac{617\nu^2}{4704} - \frac{10\,993\nu}{14\,112} - \frac{47\,009}{56\,448}\right)x^2 + \left(\frac{7\,613\,184\,941}{2\,607\,897\,600} - \frac{107}{105}\mathrm{eulerlog}_1(x)\right)x^3 + \left(\frac{6313}{5880}\mathrm{eulerlog}_1(x) - \frac{1\,168\,617\,463\,883}{911\,303\,737\,344}\right)x^4 + \mathcal{O}(x^5), \tag{C2}$$

$$\rho_{33}(x;\nu) = 1 + \left(\frac{2\nu}{3} - \frac{7}{6}\right)x + \left(\frac{149\nu^2}{330} - \frac{1861\nu}{990} - \frac{6719}{3960}\right)x^2 + \left(\frac{3\,203\,101\,567}{227\,026\,800} - \frac{26}{7}\mathrm{eulerlog}_3(x)\right)x^3 + \left(\frac{13}{3}\mathrm{eulerlog}_3(x) - \frac{57\,566\,572\,157}{8\,562\,153\,600}\right)x^4 + \mathcal{O}(x^5), \tag{C3}$$

$$\rho^J_{32}(x;\nu) = 1 + \frac{320\nu^2 - 1115\nu + 328}{270(3\nu - 1)}x + \frac{3\,085\,640\nu^4 - 20\,338\,960\nu^3 - 4\,725\,605\nu^2 + 8\,050\,045\nu - 1\,444\,528}{1\,603\,800(1 - 3\nu)^2}x^2 + \left(\frac{5\,849\,948\,554}{940\,355\,325} - \frac{104}{63}\mathrm{eulerlog}_2(x)\right)x^3 + \mathcal{O}(x^4), \tag{C4}$$

$$\rho_{31}(x;\nu) = 1 + \left(-\frac{2\nu}{9} - \frac{13}{18}\right)x + \left(-\frac{829\nu^2}{1782} - \frac{1685\nu}{1782} + \frac{101}{7128}\right)x^2 + \left(\frac{11\,706\,720\,301}{6\,129\,723\,600} - \frac{26}{63}\mathrm{eulerlog}_1(x)\right)x^3 + \left(\frac{169}{567}\mathrm{eulerlog}_1(x) + \frac{2\,606\,097\,992\,581}{4\,854\,741\,091\,200}\right)x^4 + \mathcal{O}(x^5), \tag{C5}$$

$$\rho_{44}(x;\nu) = 1 + \frac{2625\nu^2 - 5870\nu + 1614}{1320(3\nu - 1)}x + \frac{1\,252\,563\,795\nu^4 - 6\,733\,146\,000\nu^3 - 313\,857\,376\nu^2 + 2\,338\,945\,704\nu - 511\,573\,572}{317\,116\,800(1 - 3\nu)^2}x^2 + \left(\frac{16\,600\,939\,332\,793}{1\,098\,809\,712\,000} - \frac{12\,568}{3465}\mathrm{eulerlog}_4(x)\right)x^3 + \mathcal{O}(x^4), \tag{C6}$$

$$\rho^J_{43}(x;\nu) = 1 + \frac{160\nu^2 - 547\nu + 222}{176(2\nu - 1)}x - \frac{6\,894\,273}{7\,047\,040}x^2 + \mathcal{O}(x^3), \tag{C7}$$

$$\rho_{42}(x;\nu) = 1 + \frac{285\nu^2 - 3530\nu + 1146}{1320(3\nu - 1)}x + \frac{-379\,526\,805\nu^4 - 3\,047\,981\,160\nu^3 + 1\,204\,388\,696\nu^2 + 295\,834\,536\nu - 114\,859\,044}{317\,116\,800(1 - 3\nu)^2}x^2 + \left(\frac{84\,823\,8724\,511}{219\,761\,942\,400} - \frac{3142}{3465}\mathrm{eulerlog}_2(x)\right)x^3 + \mathcal{O}(x^4), \tag{C8}$$

$$\rho^J_{41}(x;\nu) = 1 + \frac{288\nu^2 - 1385\nu + 602}{528(2\nu - 1)}x - \frac{7\,775\,491}{21\,141\,120}x^2 + \mathcal{O}(x^3), \tag{C9}$$

$$\rho_{55}(x;\nu) = 1 + \frac{512\nu^2 - 1298\nu + 487}{390(2\nu - 1)}x - \frac{3\,353\,747}{2\,129\,400}x^2 + \mathcal{O}(x^3), \tag{C10}$$

$$\rho^J_{54}(x;\nu) = 1 + \frac{33\,320\nu^3 - 127\,610\nu^2 + 96\,019\nu - 17\,448}{13\,650(5\nu^2 - 5\nu + 1)}x + \mathcal{O}(x^2), \tag{C11}$$

$$\rho_{53}(x;\nu) = 1 + \frac{176\nu^2 - 850\nu + 375}{390(2\nu - 1)}x - \frac{410\,833}{709\,800}x^2 + \mathcal{O}(x^3), \tag{C12}$$

$$\rho^J_{52}(x;\nu) = 1 + \frac{21\,980\nu^3 - 104\,930\nu^2 + 84\,679\nu - 15\,828}{13\,650(5\nu^2 - 5\nu + 1)}x + \mathcal{O}(x^2), \tag{C13}$$

$$\rho_{51}(x;\nu) = 1 + \frac{8\nu^2 - 626\nu + 319}{390(2\nu - 1)}x - \frac{31\,877}{304\,200}x^2 + \mathcal{O}(x^3), \tag{C14}$$

$$\rho_{66}(x;\nu) = 1 + \frac{273\nu^3 - 861\nu^2 + 602\nu - 106}{84(5\nu^2 - 5\nu + 1)}x + \mathcal{O}(x^2), \tag{C15}$$

$$\rho^J_{65}(x;\nu) = 1 + \frac{220\nu^3 - 910\nu^2 + 838\nu - 185}{144(3\nu^2 - 4\nu + 1)}x + \mathcal{O}(x^2), \tag{C16}$$

$$\rho_{64}(x;\nu) = 1 + \frac{133\nu^3 - 581\nu^2 + 462\nu - 86}{84(5\nu^2 - 5\nu + 1)}x + \mathcal{O}(x^2), \tag{C17}$$

$$\rho^J_{63}(x;\nu) = 1 + \frac{156\nu^3 - 750\nu^2 + 742\nu - 169}{144(3\nu^2 - 4\nu + 1)}x + \mathcal{O}(x^2) \tag{C18}$$

$$\rho_{62}(x;\nu) = 1 + \frac{49\nu^3 - 413\nu^2 + 378\nu - 74}{84(5\nu^2 - 5\nu + 1)}x + \mathcal{O}(x^2), \tag{C19}$$

$$\rho^J_{61}(x;\nu) = 1 + \frac{124\nu^3 - 670\nu^2 + 694\nu - 161}{144(3\nu^2 - 4\nu + 1)}x + \mathcal{O}(x^2), \tag{C20}$$

$$\rho_{77}(x;\nu) = 1 + \frac{1380\nu^3 - 4963\nu^2 + 4246\nu - 906}{714(3\nu^2 - 4\nu + 1)}x + \mathcal{O}(x^2), \tag{C21}$$

$$\rho^J_{76}(x;\nu) = 1 + \frac{6104\nu^4 - 29\,351\nu^3 + 37\,828\nu^2 - 16\,185\nu + 2144}{1666(7\nu^3 - 14\nu^2 + 7\nu - 1)}x + \mathcal{O}(x^2), \tag{C22}$$

$$\rho_{75}(x;\nu) = 1 + \frac{804\nu^3 - 3523\nu^2 + 3382\nu - 762}{714(3\nu^2 - 4\nu + 1)}x + \mathcal{O}(x^2), \tag{C23}$$

$$\rho^J_{74}(x;\nu) = 1 + \frac{41\,076\nu^4 - 217\,959\nu^3 + 298\,872\nu^2 - 131\,805\nu + 17\,756}{14\,994(7\nu^3 - 14\nu^2 + 7\nu - 1)}x + \mathcal{O}(x^2), \tag{C24}$$

$$\rho_{73}(x;\nu) = 1 + \frac{420\nu^3 - 2563\nu^2 + 2806\nu - 666}{714(3\nu^2 - 4\nu + 1)}x + \mathcal{O}(x^2), \tag{C25}$$

$$\rho^J_{72}(x;\nu) = 1 + \frac{32\,760\nu^4 - 190\,239\nu^3 + 273\,924\nu^2 - 123\,489\nu + 16\,832}{14\,994(7\nu^3 - 14\nu^2 + 7\nu - 1)}x + \mathcal{O}(x^2), \tag{C26}$$

$$\rho_{71}(x;\nu) = 1 + \frac{228\nu^3 - 2083\nu^2 + 2518\nu - 618}{714(3\nu^2 - 4\nu + 1)}x + \mathcal{O}(x^2), \tag{C27}$$

$$\rho_{88}(x;\nu) = 1 + \frac{12\,243\nu^4 - 53\,445\nu^3 + 64\,659\nu^2 - 26\,778\nu + 3482}{2736(7\nu^3 - 14\nu^2 + 7\nu - 1)}x + \mathcal{O}(x^2), \tag{C28}$$

$$\rho^J_{87}(x;\nu) = 1 + \frac{38\,920\nu^4 - 207\,550\nu^3 + 309\,498\nu^2 - 154\,099\nu + 23\,478}{18\,240(4\nu^3 - 10\nu^2 + 6\nu - 1)}x + \mathcal{O}(x^2), \tag{C29}$$

$$\rho_{86}(x;\nu) = 1 + \frac{2653\nu^4 - 13\,055\nu^3 + 17\,269\nu^2 - 7498\nu + 1002}{912(7\nu^3 - 14\nu^2 + 7\nu - 1)}x + \mathcal{O}(x^2), \tag{C30}$$

$$\rho^J_{85}(x;\nu) = 1 + \frac{6056\nu^4 - 34\,598\nu^3 + 54\,642\nu^2 - 28\,055\nu + 4350}{3648(4\nu^3 - 10\nu^2 + 6\nu - 1)}x + \mathcal{O}(x^2), \tag{C31}$$

$$\rho_{84}(x;\nu) = 1 + \frac{4899\nu^4 - 28\,965\nu^3 + 42\,627\nu^2 - 19\,434\nu + 2666}{2736(7\nu^3 - 14\nu^2 + 7\nu - 1)}x + \mathcal{O}(x^2), \tag{C32}$$

$$\rho^J_{83}(x;\nu) = 1 + \frac{24\,520\nu^4 - 149\,950\nu^3 + 249\,018\nu^2 - 131\,059\nu + 20\,598}{18\,240(4\nu^3 - 10\nu^2 + 6\nu - 1)}x + \mathcal{O}(x^2), \tag{C33}$$

$$\rho_{82}(x;\nu) = 1 + \frac{3063\nu^4 - 22\,845\nu^3 + 37\,119\nu^2 - 17\,598\nu + 2462}{2736(7\nu^3 - 14\nu^2 + 7\nu - 1)}x + \mathcal{O}(x^2), \tag{C34}$$

$$\rho^J_{81}(x;\nu) = 1 + \frac{21\,640\nu^4 - 138\,430\nu^3 + 236\,922\nu^2 - 126\,451\nu + 20\,022}{18\,240(4\nu^3 - 10\nu^2 + 6\nu - 1)}x + \mathcal{O}(x^2). \tag{C35}$$

[1] T. Damour and A. Nagar, Phys. Rev. D **76**, 064028 (2007).
[2] T. Damour and A. Nagar, Phys. Rev. D **77**, 024043 (2008).
[3] L. Blanchet, Living Rev. Relativity **9**, 4 (2006).
[4] C. Cutler, E. Poisson, G. J. Sussman, and L. S. Finn, Phys. Rev. D **47**, 1511 (1993).
[5] E. Poisson, Phys. Rev. D **52**, 5719 (1995).
[6] T. Damour, B. R. Iyer, and B. S. Sathyaprakash, Phys. Rev. D **57**, 885 (1998).
[7] A. Buonanno and T. Damour, Phys. Rev. D **59**, 084006 (1999).
[8] A. Buonanno and T. Damour, Phys. Rev. D **62**, 064015 (2000).
[9] F. Pretorius, arXiv:0710.1338.
[10] T. Damour, A. Nagar, M. Hannam, S. Husa, and B. Brugmann, Phys. Rev. D **78**, 044039 (2008).
[11] A. Buonanno *et al.*, Phys. Rev. D **76**, 104049 (2007).
[12] L. E. Kidder, Phys. Rev. D **77**, 044016 (2008).
[13] E. Berti *et al.*, Phys. Rev. D **76**, 064034 (2007).
[14] L. Blanchet, G. Faye, B. R. Iyer, and S. Sinha, Classical Quantum Gravity **25**, 165003 (2008).
[15] H. Tagoshi and M. Sasaki, Prog. Theor. Phys. **92**, 745 (1994).
[16] T. Tanaka, H. Tagoshi, and M. Sasaki, Prog. Theor. Phys. **96**, 1087 (1996).
[17] N. Yunes and E. Berti, Phys. Rev. D **77**, 124006 (2008).
[18] T. Damour, A. Nagar, E. N. Dorband, D. Pollney, and L. Rezzolla, Phys. Rev. D **77**, 084017 (2008).
[19] L. Blanchet and T. Damour, Phys. Rev. D **46**, 4304 (1992).
[20] L. Blanchet, Classical Quantum Gravity **15**, 113 (1998).
[21] E. Poisson, Phys. Rev. D **47**, 1497 (1993).
[22] T. Damour, B. R. Iyer, P. Jaranowski, and B. S. Sathyaprakash, Phys. Rev. D **67**, 064028 (2003).
[23] K. S. Thorne, Rev. Mod. Phys. **52**, 299 (1980).
[24] E. Poisson and M. Sasaki, Phys. Rev. D **51**, 5753 (1995).
[25] M. Sasaki and H. Tagoshi, Living Rev. Relativity **6**, 2003, http://www.livingreviews.org/lrr-2003-6.
[26] K. G. Arun, L. Blanchet, B. R. Iyer, and M. S. S. Qusailah, Classical Quantum Gravity **21**, 3771 (2004).
[27] A. Nagar and L. Rezzolla, Classical Quantum Gravity **22**, R167 (2005); **23**, 4297(E) (2006).
[28] T. Damour, P. Jaranowski, and G. Schäfer, Phys. Rev. D **62**, 084011 (2000).
[29] A. Buonanno, G. B. Cook, and F. Pretorius, Phys. Rev. D **75**, 124018 (2007).
[30] L. Blanchet and T. Damour, Ann. Inst. Henri Poincaré, A **50**, 377 (1989).
[31] T. Damour and B. R. Iyer, Ann. Inst. Henri Poincaré, A **54**, 115 (1991).
[32] T. Damour, E. Gourgoulhon, and P. Grandclement, Phys. Rev. D **66**, 024007 (2002).
[33] A. Nagar, T. Damour, and A. Tartaglia, Classical Quantum Gravity **24**, S109 (2007).
[34] E. Gourgoulhon, P. Grandclement, and S. Bonazzola, Phys. Rev. D **65**, 044020 (2002).
[35] K. Uryu, F. Limousin, J. L. Friedman, E. Gourgoulhon, and M. Shibata, Phys. Rev. Lett. **97**, 171101 (2006).
[36] L. Blanchet, B. R. Iyer, and B. Joguet, Phys. Rev. D **65**, 064005 (2002).